Mechanisms of dissolved and labile particulate iron supply to shelf waters and phytoplankton blooms off South Georgia, Southern Ocean

Christian Schlosser[1,2,*], Katrin Schmidt[3,4], Alfred Aquilina[1], William B. Homoky[1,5], Maxi Castrillejo[1,6], Rachel A. Mills[1], Matthew D. Patey[1], Sophie Fielding[3], Angus Atkinson[7], and Eric P. Achterberg[1,2]

[1] Ocean and Earth Science, National Oceanography Centre Southampton, University of Southampton, SO14 3ZH Southampton, United Kingdom

[2] GEOMAR Helmholtz Centre for Ocean Research, Wischhofstr. 1-3, 24148 Kiel, Germany

[3] British Antarctic Survey, CB3 0ET Cambridge, United Kingdom

[4] School of Geography, Earth and Environmental Sciences, University of Plymouth, PL4 8AA Plymouth, United Kingdom

[5] Department of Earth Sciences, University of Oxford, OX1 3AN Oxford, United Kingdom

[6] Institut de Ciència i Tecnologia Ambientals & Departament de Física, Universitat Autònoma de Barcelona, 08193 Bellaterra, Spain

[7] Plymouth Marine Laboratory, Prospect Place, The Hoe, PL1 3DH Plymouth, United Kingdom

For submission to Biogeosciences

* Corresponding author Christian Schlosser (Email: cschlosser@geomar.de, Phone: 0049 (0) 431 600 1297)

Abstract (375 words)

The island of South Georgia is situated in the iron (Fe) depleted Antarctic Circumpolar Current of the Southern Ocean. Iron emanating from its shelf system fuels large phytoplankton blooms downstream of the island, but the actual supply mechanisms are unclear. To address this, we present an inventory of Fe, manganese (Mn) and aluminium (Al) in shelf sediments, pore waters and the water column in the vicinity of South Georgia, alongside data on zooplankton-mediated Fe cycling processes, and provide estimates of the relative dissolved Fe (DFe) fluxes from these sources. Seafloor sediments, modified by authigenic Fe precipitation, were the main particulate Fe source to shelf bottom waters as indicated by the similar Fe/Mn and Fe/Al ratios for shelf sediments and suspended particles in the water column. Less than 1% of the total particulate Fe pool was leachable surface adsorbed (labile) Fe, and therefore potentially available to organisms. Pore waters formed the primary DFe source to shelf bottom waters supplying 0.1 – 44 μmol DFe m^{-2} d^{-1}. However, we estimate that only 0.41 ± 0.26 μmol DFe m^{-2} d^{-1} was transferred to the surface mixed layer by vertical diffusive and advective mixing. Other trace metal sources to surface waters included glacial flour released by melting glaciers and via zooplankton egestion and excretion processes. On average 6.5 ± 8.2 μmol m^{-2} d^{-1} of labile particulate Fe was supplied to the surface mixed layer via faecal pellets formed by Antarctic krill (*Euphausia superba*), with a further 1.1 ± 2.2 μmol DFe m^{-2} d^{-1} released directly by the krill. The faecal pellets released by krill included seafloor-derived lithogenic and authigenic material and settled algal debris, in addition to freshly ingested suspended phytoplankton cells.

The Fe requirement of the phytoplankton blooms ~1,250 km downstream of South Georgia was estimated at 0.33 ± 0.11 μmol m^{-2} d^{-1}, with the DFe supply by horizontal/vertical mixing, deep winter mixing and aeolian dust estimated as ~0.12 μmol m^{-2} d^{-1}. We hypothesize that a substantial contribution of DFe was provided through recycling of

biogenically stored Fe following luxury Fe uptake by phytoplankton on the Fe-rich shelf. This process would allow Fe to be retained in the surface mixed layer of waters downstream of South Georgia through continuous recycling and biological uptake, supplying the large downstream phytoplankton blooms.

1. Introduction

The Southern Ocean is the largest 'High Nitrate Low Chlorophyll' (HNLC) region of the global ocean (Buesseler et al., 2004), as a consequence of low iron (Fe) supply and subsequent reduced phytoplankton growth (Buesseler et al., 2004; Tsuda et al., 2009). Iron can be supplied to surface waters of the Southern Ocean by atmospheric dust inputs (Cassar et al., 2007; Gao et al., 2001), horizontal/vertical advective and diffusive mixing processes (de Jong et al., 2012), resuspension from shelf sediments (Kalnejais et al., 2010; Marsay et al., 2014), melting of icebergs and glaciers (Raiswell et al., 2008), and hydrothermal inputs (German et al., 2016). Despite the overall HNLC status of the Southern Ocean, regions in the wake of islands feature large seasonal phytoplankton blooms; the Fe sources to these blooms are however poorly constrained (de Jong et al., 2012; Planquette et al., 2007; Pollard et al., 2009).

Downstream of the island of South Georgia intense, long-lasting phytoplankton blooms have been observed which extend hundreds of kilometres, and require an enhanced Fe supply. The blooms peak in austral summer (Borrione et al., 2013), stretch over an area of ~ 750,000 km^2 (Atkinson et al., 2001; Korb et al., 2004), and are responsible for the largest dissolved inorganic carbon deficit reported within the Antarctic Circumpolar Current (ACC) (Jones et al., 2015; Jones et al., 2012). As a consequence of the Fe fertilisation, the waters in the vicinity of South Georgia support extensive phytoplankton blooms and a large biomass of zooplankton, fish, seabirds and marine mammals, some of which are exploited commercially (Atkinson et al., 2001; Murphy et al., 2007).

South Georgia forms part of the volcanically active Scotia Arc in the Atlantic sector of the Southern Ocean and is surrounded by a broad 30 to 100 km wide shelf with an average (albeit highly variable) depth of ca. 200 m (Fig. 1). The island is situated between the Antarctic Polar Front (PF) and the Southern ACC Front (SACCF), within the general

78 northeast flow of the ACC (Meredith et al., 2005; Whitehouse et al., 2008). The ACC
79 surface waters are enriched in nitrate, phosphate and silicic acid, but strongly depleted in
80 most trace elements, notably Fe and manganese (Mn) (Browning et al., 2014). The large
81 seasonal phytoplankton blooms downstream of South Georgia are thought to be supplied with
82 Fe from the island during the passage of ACC waters (Borrione et al., 2013; Nielsdóttir et al.,
83 2012).

84 In this study we provide the first comprehensive data set of dissolved and (labile)
85 particulate Fe, Mn, and Al in sediments, pore waters, and the water column overlaying the
86 shelf and shelf edge regions of South Georgia. We also include published data on the role of
87 Antarctic krill in new Fe supply and recycling in this region (Schmidt et al., 2011; Schmidt et
88 al., 2016). We discuss differences between the various analysed trace metal fractions and the
89 supply routes of dissolved and (labile) particulate Fe, such as sedimentary pore water efflux,
90 supply of sediment derived particulate Fe to the surface mixed layer, efflux of Fe from glacial
91 melting and supply of Fe by faecal pellets of Antarctic krill. Furthermore, we discuss the
92 productivity of the bloom region to the north of South Georgia in relation to the estimated Fe
93 supply rates.
94
95 **2. Methods**
96 **2.1 Cruises and Sampling**
97 Samples were collected during three research cruises to South Georgia in 2011
98 (JR247, JC055), and 2013 (JR274). While cruises JR247 and JR274 aimed to examine the
99 pelagic shelf ecosystem by collection of predominantly water samples (and zooplankton
100 during JR247) on the northern shelf, JC055 explored solely the composition of sediments on
101 the South Georgia shelf. Cruise JR247 took place in January 2011 on RRS *James Clark*
102 *Ross*, and 14 sites on the northern shelf and shelf edge of South Georgia were visited (stations

1 – 21; Fig. 1). Suspended particles were collected on acid cleaned polycarbonate filters (1 µm pore size; Whatman) using in-situ Stand-Alone Pumping Systems (SAPS; Challenger Oceanic) attached to a Kevlar wire and deployed at 20 m, 50 m and 150 m depth (Fig. 1, red dots). The filters were rinsed with deionized water (Milli-Q; Millipore), stored at -20°C, and shipped frozen to the National Oceanography Centre Southampton (NOCS).

Subsurface seawater samples were collected by trace metal clean samplers (Ocean Test Equipment (OTE)) at 9 of the 14 SAPS locations (Fig. 1; black stars). Seawater samples were filtered using cartridge filter (0.2 µm Sartobran P300; Sartorius) into acid cleaned 125 mL low-density polyethylene (LDPE) bottles (Nalgene). Unfiltered samples were collected in 125 mL LDPE bottles for analysis of total dissolvable (TD) trace metals. Surface waters from the South Georgia shelf were collected using a tow fish deployed alongside the ship at 3 – 4 m depth. Samples were filtered in-line using a cartridge filter (0.2 µm Sartobran P300; Sartorius) and dispensed in acid washed 125 mL LDPE bottles. Unfiltered surface seawater samples were also collected and dispensed in acid washed 125 mL LDPE bottles. All seawater samples were acidified on-board with ultra clean HNO_3 (15 M UpA grade, Romil) to pH 1.7 (22 µmol H^+ L^{-1}). For a more detailed description of all sample-handling procedures, please see Supplementary Text S1.

In January and February 2013, RRS *James Clark Ross* cruise JR274 revisited South Georgia and collected surface seawater samples covering the shelf, shelf-edge, and open ocean areas around the island. Dissolved and TD trace elements in surface seawater samples were collected using the tow fish and treated similarly to samples from JR247. For a more detailed description of all sample-handling procedures, please see Supplementary Text S1.

During the RRS *James Cook* cruise JC055 in February 2011, a megacorer (Bowers and Connelly type) was used to collect surface sediment and pore water samples on the southern side of South Georgia (there was no opportunity to sample the northern side of the

island). Cores representing the intact sediment – water interface were retrieved from three sites on the southern shelf, at water depths of ca. 250 m (S1 – S3) (Fig. 1, blue hexagons). Pore waters were separated by centrifugation under N_2 atmosphere and filtered using cellulose nitrate syringe filters (0.2 μm pore size; Whatman (Homoky et al., 2012). Conjugate sediments were freeze dried on board and stored at room temperature. A more detailed description of sediment and pore water sample-handling procedures is provided in Supplementary Text S2.

Krill faecal pellets were obtained during on-board krill incubations performed during JR247. Incubations were performed in darkness in the laminar flow cabinet at ambient surface layer temperature. The krill were incubated in filtered seawater from the tow fish for up to ~3 h immediately after capture, so that pellets obtained derived from material ingested in situ. These incubations and their results are described in more detail in Schmidt et al. (2016).

2.2 Trace metal analysis in suspended particles and krill faecal pellets

The labile trace metal fraction of suspended particles (SAPS) and krill faecal pellets, was remobilized using a 25% acetic acid solution (glacial SpA, Romil) following Planquette et al. (2011). The labile trace metal fraction is hereafter referred to as the leachable trace metal fraction (L). The remaining particles were digested on a hot plate applying a mixture of aqua regia and hydrogen fluoride (Planquette et al., 2011). This fraction will be referred to as the refractory fraction (R). The particulate trace metal fraction (P) is the sum of leachable (L) and refractory (R). All samples were analysed by collision cell inductively coupled plasma - mass spectrometry (ICP-MS) (ThermoFisher Scientific, XSeriesII). For more detailed description of measured certified reference material see Supplementary Text S1.

153 **2.3 Trace metal analysis of seawater**

154 The filtered and unfiltered seawater samples were stored for a period of 12 months
155 prior to analysis. Concentrations of dissolved and total dissolvable Fe, Mn, and Al in
156 seawater were determined by off-line pre-concentration and isotope dilution / standard
157 addition ICP-MS (ThermoFisher Scientific Element2 XR) according to Rapp et al. (2017).
158 For a more detailed description of the method and measured reference materials see
159 Supplementary Text S1.

160

161 **2.4 Trace metal analysis of pore waters and sediments**

162 Sub-samples of the bulk, homogenized sediments were fully dissolved following an
163 aqua regia and combined hydrofluoric/perchloric acid digestion method following Homoky et
164 al. (2011). The acid digests and pore waters were analysed by ICP-optical emission
165 spectrometry (OES) (Perkin Elmer Optima 4300DV). For a more detailed description of the
166 method and measured reference materials see Supplementary Text S2.

167

168 **3. Results & Discussion**

169 **3.1 Supply routes of suspended particulate Fe, Mn, and Al**

170 To avoid confusion, we will now define the terms biogenic, lithogenic, and authigenic
171 particles, as they will be used frequently in the following sections. Biogenic particles refer to
172 suspended organic particles, living and dead, such as phytoplankton cells. Lithogenic
173 particles comprise mineral fragments, such as glacial flour and sediment particles.
174 Authigenic particle include surface-scavenged trace metals and secondary minerals, such as
175 amourphous FeO(OH) (e.g. goethite), that are formed in seawater and because of their age
176 are insoluble to weak acid leaches (e.g. 25% acetic acid solution).

177 3.1.1 Characterization of (the two) particulate trace metal fractions

178 Two different particulate fractions were obtained from samples collected during
179 JR247; a particulate fraction from suspended particles collected using 1 µm pore size SAPS
180 filters (P) and a leachable particulate fraction from unfiltered acidified seawater samples
181 (LP_{Un}) collected at the same depth. LP_{Un} was calculated following Eq. (1):

182 LP_{Un} = total dissolvable (TD; unfiltered) – dissolved (D; 0.2 µm filtered) (1)

183 Because of the different sampling approaches (SAPS vs. OTE water samplers), filter sizes
184 (>1 µm for SAPS vs. >0.2 µm for dissolved seawater) and digestion procedures (aqua regia +
185 HF for SAPS particles vs. water sample storage at pH 1.7 [22 µmol H^+ L^{-1}]), concentrations
186 of LP_{Un} and P differed, but showed similar distribution patterns in the water column (Fig. 2
187 and S1, Table 1 and 2). The concentrations of Fe, Mn and Al in the LP_{Un} fraction ($LP_{Un}Fe$,
188 $LP_{Un}Mn$, $LP_{Un}Al$) were usually slightly lower than the particulate fraction from suspended
189 particles (PFe, PMn, PAl). The LP_{Un} of unfiltered seawater samples corresponded to ~ 63 ± 4
190 % of the PFe, 83 ± 11% of the PAl and nearly 100 ± 10% of the PMn fractions obtained by
191 SAPS. The average LP_{Un} trace metal ratios ($LP_{Un}Fe$/ $LP_{Un}Mn$ = 33.07 ± 3.45 (1 σ) and
192 $LP_{Un}Fe$/ $LP_{Un}Al$ = 0.65 ± 0.10 (n=69)), were about half of the elemental ratios of suspended
193 particles obtained by SAPS (PFe/PMn = 68.0 ± 0.6 and PFe/PAl = 1.251 ± 0.042 (n=42) (Fig.
194 3; Table 1, 2 and 3)).

195 The lower concentrations of Fe and Al and the reduced elemental ratios in the LP_{Un}
196 compared to the P fractions suggests that an unknown fraction of particulate Fe and Al in
197 seawater was not leached during the acidification procedure at pH 1.7 over 12 months.
198 However, since P and LP_{Un} displayed similar trends with depth (Fig. 2 and S1), LP_{Un} was
199 used in sections 3.1.3 and 3.3 as an indicator for the abundance of particulate trace metals at
200 locations where particulate samples could not be retrieved by SAPS, e.g. in surface waters
201 collected by the tow fish and depths greater than 150 m.
202

3.1.2 Suspended particulate trace metals in the water column

Concentrations of PFe, PMn and PAl in the water column ranged from 0.87 – 267 nmol L^{-1}, 0.01 – 3.85 nmol L^{-1}, and 0.60 – 195 nmol L^{-1}, respectively (Fig. 2, Table 2). Concentrations of $LP_{Un}Fe$, $LP_{Un}Mn$ and $LP_{Un}Al$ ranged from 1 – 118 nmol L^{-1}, 0.01 – 100 nmol L^{-1}, and 1 – 141 nmol L^{-1}, respectively (Fig. 2, Table 1). Below the isopycnal density layer 27.05 kg m^{-3}, located at ~50 – 70 m depth, P and LP_{Un} increased with depth and showed a maximum near the seafloor of e.g. 207 nmol L^{-1} for PFe and 112 nmol L^{-1} for $LP_{Un}Fe$ (#17, Table 2). Most sites on the shelf (bottom depth ≤ 260 m; #9/10, #13, #14, #17, and #21) showed seafloor maxima, in agreement with other shelf studies. For example, Milne et al. (2017) reported concentrations of up to 140 nmol L^{-1} for PFe and 800 nmol L^{-1} for PAl in bottom waters on the west African shelf, and Chase et al. (2005) showed bottom water maxima of up to 400 nmol L^{-1} for $LP_{Un}Fe$ off the Oregon coast.

Strong linear relationships between elements were observed for suspended particles (SAPS) obtained from above and below the 27.05 kg m^{-3} isopycnal, with elemental ratios of PFe/PMn = 68.0 ± 0.6, PFe/PAl = 1.25 ± 0.04 and PMn/PAl = 0.0171 ± 0.0041 (n=42) (Fig. 3, Table 2 and 3). These elemental ratios were higher than those reported for the earth's crust (Fe/Mn = 58.0, Fe/Al = 0.2, Mn/Al = 0.0035 (Wedepohl, 1995)) and sediment samples collected to the south of the island (mean sediment surface layer of S1, S2, S3; SFe/SMn = 51.5 ± 2.4, SFe/SAl = 0.34 ± 0.02, SMn/SAl = 0.0066 ± 0.0002 (Fig. 4, Table 3 and 4)), suggesting that the suspended particles were more enriched in Fe than crustal and lithogenic particles (Table 3).

The Fe/Mn ratios among different phytoplankton species show strong variations but are typically much lower (Fe/Mn ~ 1.7 (Ho et al., 2003)), with also lower Fe concentrations than lithogenic (sediment) particles (cellular Fe concentration of phytoplankton ~ 0.7 mmol kg^{-1} (Ho et al., 2003); upper crust ~ 550 mmol kg^{-1} (Wedepohl, 1995)). A prevalence of

biogenic particles in the suspended particle pool would be expected to result in reduced PFe/PMn ratios in our SAPS samples to values less than 51.5 as was observed in the sediments.

It is most likely that authigenic Fe precipitation (e.g. DFe was scavenged onto sediment particles) increased the Fe to Al (and Fe to Mn) ratio of suspended particles (PFe/PAl = 1.25; PFe/PMn = 68.0) compared to sediment particles (SFe/SAl = 0.34; SFe/SMn = 51.5). At seawater pH (~pH 8), dissolved Fe(III) is rapidly hydrolysed to soluble $Fe(III)(OH)_3$ (< 0.02 µm) which readily accumulates as nanometer sized colloids (0.02 – 0.2 µm) (Liu and Millero, 2002) and particles (> 0.2 µm) (own observation). It has been also shown that both soluble and colloidal Fe are attracted by charged surfaces (organic and inorganic particle surfaces), a process that removes DFe and simultaneously increases the amount of particulate Fe in seawater over time (Schlosser et al., 2011).

A range of mechanisms delivers suspended particles to the surface waters. These transport mechanisms will be discussed in the following section.

3.1.3 Glacial outflow and zooplankton feeding activity

While most stations on the shelf showed bottom water maxima of particulate metals, at three sampling sites located on the shelf (#18) and shelf edge (#15/16 and #19/20), the particulate trace metal concentrations featured maxima in the top 100 m of the water column (Fig. 2 and 5). At site #19/20, ca. 100 km away from the coast with a water depth of 1.741 m, the PFe concentration at 20 m depth was 97 nmol L^{-1}, similar to $LP_{Un}Fe$ (Fig. 5). The elemental ratio PFe/PAl of these samples (e.g. 1.01 for site #19/20, 20 m depth) were close to the average ratio (PFe/PAl = 1.25), indicating that lithogenic and authigenic Fe dominated the suspended particulate pool in these surface waters.

The surface water maxima of trace metals could have two supply routes: 1) lateral transport of waters containing lithogenic and authigenic particles from shallow island shelf sediments, and 2) transport of glacial particles following melt processes. The reduced salinities (~33.3 PSU) recorded in surface waters in Cumberland Bay and ~50 km offshore of South Georgia (~33.8) (Fig. 6(c) and S2) provide an indication of glacial outflow, melting of icebergs and run-off of melt water streams. Enhanced $LP_{Un}Fe$ concentrations of 2.2 µmol L^{-1} in low salinity surface waters inside Cumberland Bay, are indicative of a meltwater source (LP_{Un} concentration used as only water samples from the tow fish available). The $LP_{Un}Fe$ concentration decreased strongly with increasing distance from the coast, and exhibited an abrupt reduction to 1 – 5 nmol Fe L^{-1} at the shelf edge ~ 100 km offshore. A similar distribution pattern was observed for $LP_{Un}Mn$ (Fig. 6(d)) and $LP_{Un}Al$ (not shown), for cruises JR247 and JR274. Glacial melt has been reported as an important source of particulate material in the vicinity of the Antarctic Peninsula (de Jong et al., 2012). For example, Gerringa et al. (2012) documented elevated total dissolvable Fe concentration of up to 106 nmol L^{-1} near the Pine Island Glacier in the Amundsen Sea, and Raiswell et al. (2008) estimated that per year 1.6 Gmol nanoparticulate Fe, associated to lithogenic particles, are delivered to the Southern Ocean by melting ice.

Locally elevated particulate metal concentrations in surface waters may also be related to production of faecal pellets by swarms of Antarctic krill (Schmidt et al., 2016). High abundances of Antarctic krill were estimated from acoustic backscattering observations (Fielding et al., 2014), and large numbers of faecal pellets were observed on the SAPS filters during cruise JR247. The stomach content of Antarctic krill contained up to 90% sediment particles by volume, an observation that was attributed to filter feeding by these organisms on phytoplankton and seabed detritus, with incidental ingestion of deep ocean sediments (Schmidt et al., 2011) and glacial flour (Schmidt et al., 2016). Krill thus take up lithogenic

277 (sediment) particles and transfer these into the surface ocean through the egestion of faecal
278 pellets (Schmidt et al., 2016). The trace metal contents of krill faecal pellets collected during
279 on-board incubation experiments during JR247 ranged from 0.88 – 67.14 µg Fe mg^{-1} dry
280 weight (n = 27) (Table 5) (Schmidt et al. 2016). The molar ratio PFe/PAl = 0.48 ± 0.07 and
281 PMn/PAl = 0.0069 ± 0.001 of the faecal pellets was similar to those for sediment particles
282 (SFe/SAl = 0.34 ± 0.02 and SMn/SAl = 0.0066 ± 0.001; Table 1, 2, 3 and 4), indicating that
283 Fe in krill faecal pellets was predominately associated with lithogenic (sediments) and/or
284 glacial flour particles, as also reported by Schmidt et al. (2016). In contrast, the molar ratio
285 PFe/PMn = 70.65 ± 8.22 of faecal pellets was higher than that of sediments, SFe/SMn = 51.5
286 ± 2.4, but just slightly higher than that of suspended SAPS particles, PFe/PAl = 68.0 ± 0.6.
287 The observed variability in the PFe/PAl and PFe/PMn ratio in the various particle pools is
288 therefore a consequence of different amounts of lithogenic and authigenic particles.
289
290 **3.2 Supply routes of dissolved Fe, Mn, and Al**
291 Concentrations of DFe, DMn, and DAl in the water column showed strong variations
292 and ranged from ~ 0.1 – 25.9 nmol L^{-1}, 0.3 – 19.6 nmol L^{-1} and 0.1 – 18.4 nmol L^{-1},
293 respectively (Fig. 2, 5 and 7), with highest values in the surface waters in Cumberland Bay,
294 and lowest beyond the shelf break (Fig. 6). Dissolved Fe concentrations from this study are
295 in agreement with reported DFe near the Antarctic Peninsula (0.6 – 14.6 nmol L^{-1} (de Jong et
296 al., 2012)) and Crozet Islands (0.1 – 2.5 nmol L^{-1} (Planquette et al., 2007)). Sources and
297 sinks of dissolved trace metals, and their distribution in the water column are discussed in the
298 following sections.
299
300 3.2.1 Supply from sediment pore waters

Elevated pore water concentrations of Fe and Mn (Fe_{PW} and Mn_{PW}) were observed in sediments from the southern shelf sites at water depths of around 250 m, and ranged from 0.5 – 110 μmol L^{-1} for Fe and 0.1 – 2 μmol L^{-1} for Mn (Fig. 7 and Table S2). The down-core distributions of Fe_{PW} and Mn_{PW} were consistent with microbial dissimilatory Mn and Fe reduction during organic matter oxidation (Canfield and Thamdrup, 2009), and thus concentrations were elevated at defined depth horizons controlled by their redox potential (Eh) (Bonneville et al., 2009; Raiswell and Canfield, 2012). The Fe_{PW} and Mn_{PW} concentrations near the sediment-seawater interface were used to calculate fluxes of Fe and Mn to bottom waters following diffusion of reduced Fe and Mn species across an oxygenated layer in surface sediments. These calculations were performed following Boudreau and Scott (1978) and Homoky et al. (2012), and are described in detailed in the Supplementary Text S3 and Table S1. We are aware that our calculated fluxes represent minimum estimates of pore water efflux, which under natural conditions is supplemented by advection due to bioirrigation, bioturbation, and bottom water currents (Homoky et al., 2016). In addition, sediment cores were collected on the southern shelf, while seawater and particulate samples were collected on the northern shelf side. The benthic Fe fluxes for the southern shelf maybe lower than those on the northern shelf, as an elevated primary productivity and enhanced particle export on the northern side will result in enhanced bacterial respiration, which reduces Eh and promotes the dissolution of Fe oxides with subsequent release of Fe into bottom waters.

Notwithstanding the above issues, we calculated substantial benthic fluxes from sediment pore waters to bottom waters on the southern shelf for Fe_{PW} of <0.1 to 44.4 μmol m^{-2} d^{-1} and Mn_{PW} of 0.6 to 4.1 μmol m^{-2} d^{-1}. The upper flux values for Fe are comparable to those reported for dysoxic and river-dominated continental margins (3.5 – 55 μmol m^{-2} d^{-1} (Homoky et al., 2012)), seasonal maxima of temperate and oxic shelf seas (23 – 31 μmol m^{-2}

d^{-1} (Klar et al., 2017)), and shelf sediments off the Antarctic Peninsula (1.3 – 15.5 μmol m^{-2} d^{-1} (de Jong et al., 2012)). The Mn fluxes were relatively low for shelf environments, with for example fluxes of 70 – 4450 μmol m^{-2} d^{-1} reported for Baltic and Black Sea sediments (Pakhomova et al., 2007)). The Fe pore water fluxes from the South Georgia shelf sediments, which extend over an area of ca. 40,000 km^2, indicate that these may serve as an important year-round source to overlying waters, totalling 4 to 1,728 kmol DFe d^{-1} and 25 to 164 kmol DMn d^{-1}.

Benthic release of trace metal enriched pore waters shaped the distributions of dissolved trace metals in bottom waters on the shelf. Concentrations of DFe, DMn, and DAl were enhanced at isopycnals > 27.05 kg m^{-3} (e.g. DFe up to 7.70 nmol L^{-1} at site #21, Table 1) compared to surface waters (e.g. DFe as low as 0.30 nmol L^{-1} at site #13, Table 1; Fig. 2 and 7). Trace metal enriched bottom waters were also observed at sites #13, #14, #17 and #18 (Fig. 2). The molar DFe/DMn ratios in oxygenated bottom waters varied between 1.1 – 3.5 and were thus similar to pore waters near the sediment-seawater interface (0 – 1 cm depth, Fe_{PW}/Mn_{PW} = 2.2 ± 1.0; Fig. 7). The similar trace metal ratios suggest that Fe and Mn in enriched pore waters crossed the sediment-bottom water interface and accumulated in shelf bottom waters.

To determine the vertical DFe fluxes from near bottom to surface waters we employed a method outlined by de Jong et al. (2012), and calculated both the advective and diffusive flux terms, which are not affected by the benthic Fe and Mn fluxes. We included the advective term in our calculations, because it has been shown that internal waves that cross shallow topographies and wind shear stress produces strong turbulence that facilitate Eckman upwelling (vertical advection) on the shelf (Kurapov et al., 2010; Moore, 2000; Wolanski and Delesalle, 1995). Applying literature values from the Southern Ocean for vertical diffusivity (K_Z = 1 x 10^{-4} m^2 s^{-1} (Charette et al., 2007)) and advective velocity (w =

351 1.1 x 10^{-6} m s^{-1} (de Jong et al., 2012)), an average vertical DFe flux on the shelf of 0.41 ±
352 0.26 µmol m^{-2} d^{-1} from subsurface waters into the surface mixed layer was estimated
353 (Supplementary Text S4). The surface mixed layer depth was determined by a density
354 criteria (~0.03 kg m^{-3} (de Boyer Montégut et al., 2004)) and was located at ~50 m depth.
355 About 38% of the DFe flux was related to Ekman upwelling (advective term) and 62% to the
356 diffusive flux. This vertical flux is at the lower end of the calculated benthic flux from this
357 study (Fe_{PW} < 0.1 to 44.4 µmol m^{-2} d^{-1}), and agrees with values reported for other Southern
358 Ocean shelf regions near the Antarctic Peninsula (within 20 – 70 km from the coast: ~ 2.7 ±
359 3.4 µmol m^{-2} d^{-1} (de Jong et al., 2012)) and the Crozet Islands (only diffusive flux of 0.06
360 µmol m^{-2} d^{-1} (Planquette et al., 2007)).
361
362 3.2.2 DFe supply from the leachable fraction of particles
363 The analytical protocol for the analysis of SAPS-collected particulate material allows
364 separate estimation of the refractory and leachable fractions of trace elements (R and L,
365 respectively). The R fraction of the suspended matter is considered to include silicates and
366 aged oxide minerals, while the L fraction represents predominantly fresh oxyhydroxides,
367 biogenic material and loosely bound surface associated elements which are readily
368 remobilized using leaching procedures (Berger et al., 2008).
369 Concentrations of LFe, LMn and LAl in the water column showed strong variations,
370 ranging from a few picomoles to several nanomoles L^{-1} (Table 2). On average, LFe and LAl
371 concentrations at 150 m depth (~ 1.3 nmol LFe L^{-1} and ~0.95 nmol LAl L^{-1}) were
372 significantly higher than at 20 and 50 m, LFe = 0.3 nmol L^{-1} (student t-test: t[0.95;28] =
373 1.725 [1.703]; t[confidence level; n-1]); LAl = 0.43 nmol L^{-1} (student t-test: t[0.90;28] =
374 1.383 [1.313]). The LMn concentrations did not vary strongly and remained near constant
375 throughout the top 150 m (LMn = 8.9 pmol L^{-1} {student t-test: [0.65;28] = 0.400 [0.390]}).

The average contribution of L to the particulate pool P (R+L), was low; 0.83 ± 1.13% for Fe, 2.55 ± 1.58% for Mn and 2.42 ± 1.32% for Al (Table 2). A study conducted in the North Pacific near the Columbia River outflow, reported considerably higher L fractions (e.g. 6.6±3.0% of Fe, 78.7±14.0% of Mn, 6.3±2.0% of Al (Berger et al., 2008)), which was attributed to enhanced biogenic particle levels in the low salinity waters of the river (Berger et al., 2008). In contrast, results from our study showed that particulate trace metals predominately had a refractory component (R), indicating that Fe, Mn, and Al was mainly incorporated in mineral structures unaffected by a weak acid leach (e.g. aged oxyhydroxides and alumosilicates).

A weak linear relationship between R and L was observed for Fe (R^2 = 0.57, n = 41), Mn (R^2 = 0.64, n = 41) and Al (R^2 = 0.63, n = 41) (Supplementary Fig. S3 and S4), indicating that the L fraction included mainly lithogenic and authigenic (e.g. scavenged) Fe, Mn and Al and not much LFe was incorporated in biogenic particles. The scavenging of dissolved trace metals by charged particle surfaces is established (Homoky et al., 2012; Koschinsky et al., 2003), but how well Fe and other trace metals can be remobilized from marine particle surfaces and which process may modify their availability over time is not yet well constrained (Achterberg et al., 2018; Fitzsimmons and Boyle, 2014; Milne et al., 2017).

For instance, scavenged Fe is reported to exchange with DFe in the water column of the tropical and high latitude North Atlantic (Achterberg et al., 2018; Fitzsimmons and Boyle, 2014; Milne et al., 2017). In addition, recent work has concluded that zooplankton grazing and the production of faecal pellets remobilizes DFe from lithogenic and biogenic particles (Giering et al., 2012; Schmidt et al., 2016). In contrast, freshly produced inorganic Fe(III) oxyhydroxide (FeOOH * nH_2O) precipitates in seawater are accessible but are subject to chemical and structural conversions that lead to less leachable Fe with time (Yoshida et al., 2006).

401

402 3.2.3 DFe supply from Antarctic krill

403 Elevated dissolved trace metal concentrations in the top 200 m of the water column
404 coincided with elevated particulate trace metal concentrations at sites #11/12, #15/16, #18,
405 and #19/20 (Fig. 2, 5, and 7). The SAPS filters from these stations contained a high load of
406 krill faecal pellets. To elucidate the relationship between dissolved trace metal
407 concentrations and the local abundance of Antarctic krill and their faecal pellets, krill were
408 caught and incubated on-board the vessel as described in Schmidt et al. (2016).

409 Antarctic krill excretion rates of DFe were variable, relating positively to the extent
410 of recent ingestion of diatoms. However, on average krill released ~2.0 ± 1.9 nmol DFe
411 individual^{-1} d^{-1} (Schmidt et al., 2016). By applying a mean krill abundance of 465 ± 588
412 individuals m^{-2}, estimated from acoustic backscattering measurements (Fielding et al., 2014),
413 krill excreted 1.1 ± 2.2 µmol DFe m^{-2} d^{-1} into the top 300 m of the water column (Schmidt et
414 al., 2016). In addition, krill produced ca. 1.8 ± 1.6 mg of faecal pellets per individual per day,
415 containing ca. 0.30 ± 0.33 µmol Fe mg^{-1}. Particle leaches performed on those faecal pellet
416 samples with 25% acetic acid showed that on average 2.5 ± 2.1% (9.3 ± 13.3 nmol Fe mg^{-1})
417 of the total Fe in these pellets could be remobilised (Table 5), which would equate to a
418 production of 14 ± 24 nmol LFe ind^{-1} d^{-1}. By multiplying the mean LFe by the ambient krill
419 density used above, we calculate a LFe flux of 6.5 ± 8.2 µmol m^{-2} d^{-1} from the faecal pellets
420 to the water column.

421 Since krill are mobile animals, questions remain over where the major part of the LFe
422 flux occurs, and what the fate of this Fe source is. Highest krill abundances were recorded
423 generally (but not exclusively) in the top 100 m layer (Fielding et al., 2014), and hence a
424 large proportion of this LFe flux from krill is likely to occur in the upper waters.
425 Notwithstanding our current uncertainties over the depths of origin and fate, the LFe flux

426 from krill faecal pellets and the release of DFe were on average an order of magnitude higher
427 than estimated vertical diffusive and advective DFe fluxes, with other grazers, such as
428 copepods and salps, adding to the recycled flux estimates. This illustrates the importance of
429 zooplankton-mediated-Fe-cycling, in agreement with previous studies (Hutchins and Bruland,
430 1994; Sato et al., 2007).

431 The experimental set-up did not allow us to establish the origin of the Fe released by
432 krill, being both "recycled" Fe from biogenic material and "new" Fe from lithogenic (and
433 authigenic) material. However, Schmidt et al. (2016) concluded that zooplankton gut passage
434 mobilizes lithogenic Fe, and showed that there are strong spatial patterns in the organic and
435 lithogenic make-up of faecal pellets. This included an exponential decline in the quantity of
436 lithogenic particles in krill stomachs with distance from sources of glacial flour on the
437 northern South Georgia coast. For instance, the lithogenic content at one site on the shelf
438 contributed ~90% of stomach content volume suggesting that a large quantity of the
439 accessible Fe was remobilized from those inorganic particles.

440

441 **3.3 Off-shore transport of trace metal enriched water masses**

442 Along a W – E transect (Fig. 1; #14 via # 13 to #11/12), lateral water mass transport
443 carried suspended particles offshore. Because of the small size of the SAPS particulate data
444 set (two data points), we considered the LP_{Un} fraction for this transect (Fig. 1). Indeed,
445 elevated concentrations of the P and LP_{Un} metal fractions were observed in subsurface waters
446 that had been in recent contact with the shelf. These metal-enriched waters, detected at the
447 eastern shelf edge site #11/12 between 200 and 400 m water depth (Fig. 1 and 4), exhibited
448 similar temperature and salinity signatures to shelf bottom waters. Furthermore, the
449 elemental ratios of the LP_{Un} fraction in these waters were similar to the particles in the surface
450 sediments (S1, S2, and S3) and the resuspended particles in the bottom boundary layer (#13

451 and #14) on the shallow shelf (Fig. 4). A similar distribution was also found for the P
452 fractions, but limited to site #13 and #14, as SAPS were not deployed below 150 m at the
453 shelf edge site #11/12.

454 The $LP_{Un}Fe$ concentration decreased with distance from the island to offshore: from
455 site #14 at 200 m depth ($LP_{Un}Fe$ = 82.26 nmol L^{-1}; water depth = 255 m) to site #13 at 100 m
456 depth ($LP_{Un}Fe$ = 34.06 nmol L^{-1}; water depth = 130 m) to site #11/12 between 200 and 400 m
457 depth ($LP_{Un}Fe$ ~ 10.18 nmol L^{-1}; water depth = 750 m) (Fig.4 and Table 1). A similar
458 decrease was observed for the SAPS Fe data: from site #14 at 150 m depth (PFe = 31.12
459 nmol L^{-1}) to site #13 at 100 m depth (PFe = 10.23 nmol L^{-1}). The decrease of PFe and
460 $LP_{Un}Fe$ with increasing distance to the coast is in agreement with previous observations for
461 the Western Subarctic Pacific (Lam and Bishop, 2008), which reported elevated LFe
462 concentrations in the range of 0.6 to 3.8 nmol L^{-1} in subsurface waters between 100 and 200
463 m depth along the Kamchatka shelf and related this observation to offshore water mass
464 transport. However, we assume that particles in the deep particulate Fe maximum are not
465 transported over very large distances, due to their tendency to sink, and thus do not
466 significantly contribute to the offshore Fe supply (section 3.4).

467 Consistent with the observed P and LP_{Un} distributions, elevated dissolved metal
468 concentrations at depths between 200 and 400 m at site #11/12 indicated that trace metal
469 enriched shelf bottom waters were transported offshore (Fig. 7). However, dissolved trace
470 metal concentrations were more variable than P and LP_{Un}, and in case for DMn were highest
471 at depths at shelf edge site #11/12. Notwithstanding the above issue, for horizontal flux
472 calculations we used the entire DFe data set for water depths between 100 and 400 m.
473 Average DFe concentrations in this depth range were highly variable and did not follow an
474 exponential or power law function with distance from the coast (Supplementary Fig. S5),

475 which is necessary to determine scale length and horizontal diffusivity (K_h) (de Jong et al.,
476 2012). As a result, horizontal flux calculations from the data could not be executed.
477 The distribution of dissolved trace metals in surface waters indicated that there was a
478 limited transfer of DFe beyond the shelf break into the bloom region. Surface samples
479 showed that DFe concentrations were strongly enriched in surface waters on the shelf (0.3 –
480 25.9 nmol L^{-1}, Fig. 6(b)), while DFe concentrations beyond the shelf break decreased
481 abruptly to concentrations < 0.2 nmol L^{-1} (Fig. 6(b)). This indicates that DFe was quickly
482 removed from ACC surface waters following passage of the island. However, previous
483 studies in the region suggest DFe transfer beyond the shelf break of South Georgia (Borrione
484 et al., 2013; Nielsdóttir et al., 2012). Nielsdóttir et al. (2012) reported surface waters
485 downstream the island shelf with up to 2 nmol DFe L^{-1}, with seasonal variations and highest
486 concentrations during austral summer in January/February 2008. Dissolved Fe data from
487 JR247 (2011) and JR274 (2012) were also obtained during the summer season, but indicated
488 rapid reduction in concentrations through mixing with DFe depleted ACC water, biological
489 uptake and/or particle scavenging (authigenic precipitation).
490
491 **3.4 Iron budget in the bloom region**
492 Large seasonal phytoplankton blooms downstream of South Georgia recorded by
493 earth observing satellites are initiated by Fe supplied by the South Georgia island/shelf
494 system during the passage of ACC waters (Fig. 1) (Borrione et al., 2013; Nielsdóttir et al.,
495 2012). Based on our study, the main DFe sources during this passage of the ACC were
496 benthic release and vertical mixing, release of DFe from krill and krill faecal pellets, and
497 supply of particles from run-off and glacial meltwater. In the following sections we will
498 discuss the strength of each DFe source in the bloom region ca. 1,250 km downstream of the
499 island and estimate how much DFe is required to stimulate the elevated primary productivity

in that region. Because of the lack of observational data for the region, this part of the study combines literature values from different Southern Ocean studies. This approach contains large uncertainties that are discussed in detail in Section 3.4.6 Budget uncertainties.

3.4.1 Phytoplankton Fe requirements in the phytoplankton bloom region

The surface ocean in the vicinity of South Georgia during the austral summer features strongly elevated biomass production (Gilpin et al., 2002) and represents the largest known CO_2 sink in the ACC (12.9 mmol C m^{-2} d^{-1} (Jones et al., 2012)). The Fe requirements of the phytoplankton community in austral summer within the bloom that reaches several hundred kilometres downstream the island were determined by combining satellite-depth integrated net primary production data derived from a phytoplankton pigment adsorption (α_{ph})-based model (62 ± 21 mmol C m^{-2} d^{-1} (Ma et al., 2014)) over the period of 2003-2010 with an average intracellular Fe/C ratio obtained from five Southern Ocean diatom species (5.23 ± 2.84 µmol Fe mol^{-1} C (Strzepek et al., 2011)). This approach yielded an approximate Fe requirement of 0.33 ± 0.11 µmol DFe m^{-2} d^{-1} for the phytoplankton community (Fig. 8). For a more detailed description of the applied values and calculations see Supplementary Text S4.

3.4.2 Horizontal and vertical mixing

De Jong et al. (2012) reported that horizontal and vertical advective, diffusive (diapycnal) and deep winter mixing downstream (1,250 – 1,570 km) of the Antarctic Peninsula (between 51°S and 59°S) supplied DFe to the surface waters in quantities that exceeded the DFe requirement of primary producers during austral summer (0.13 ± 0.04 µmol DFe m^{-2} d^{-1}). In their study region, de Jong et al. (2012) determined that ~ 0.30 ± 0.22 µmol DFe m^{-2} d^{-1} were supplied by horizontal and vertical fluxes, of which 91% of the vertical flux were attributed to Ekman upwelling (advective term), and 43% of the entire DFe

525 flux was supplied by deep winter mixing. Tagliabue et al. (2014) reported similar model
526 estimates for the region that is located south of the Polar Front and characterized by strong
527 Ekman upwelling and winter entrainment.
528 For the bloom region downstream of South Georgia, model calculations by Tagliabue
529 et al. (2014) indicated that less than 0.0003 µmol DFe m^{-2} d^{-1} were supplied by diapycnal
530 mixing, and ~ -0.0027 µmol DFe m^{-2} d^{-1} were removed by Ekman down-welling. For the
531 vertical flux component, this yields an overall loss of DFe of ~ -0.002 µmol DFe m^{-2} d^{-1}
532 (0.0003 + (-0.0027)) in the bloom region north of South Georgia (Fig. 8).
533 Because the sampling in our study was not suitable for calculations of the horizontal
534 flux, we applied the horizontal flux estimates from de Jong et al. (2012) for our own Fe
535 budget. For a region ca. 1,250 km downstream of a source, calculations according to de Jong
536 et al. (2012) sugest that ca. 0.11 ± 0.03 µmol DFe m^{-2} d^{-1} are supplied to the bloom region by
537 horizontal advection and diffusion (Fig. 8).
538
539 3.4.3 Deep winter mixing
540 The entrainment of new DFe during winter represents an important Fe source to
541 surface waters in the Southern Ocean (de Jong et al., 2012; Tagliabue et al., 2014). Elevated
542 DFe concentrations in subsurface waters support primary production in the austral spring
543 following entrainment by deep winter mixing. Model estimates showed that DFe supplied by
544 winter mixing, together with diapycnal mixing, matches the Fe requirements at most low
545 productivity sites in the Southern Ocean. However, deep winter mixing at the highly
546 productive sites north of South Georgia supplies only ~ 0.011 µmol m^{-2} d^{-1} (Tagliabue et al.,
547 2014) (Fig. 8). Later in the season primary productivity in surface waters is considered to rely
548 strongly on Fe derived from recycling of biogenic material (Boyd et al., 2015).
549

550 3.4.4 Dust deposition

551 Dissolved Fe supplied by the deposition of aeolian dust is considered to be an
552 important source to the Southern Ocean (Conway et al., 2015; Gabric et al., 2010; Gassó and
553 Stein, 2007). Aeolian flux model estimates, supplied by Borrione et al. (2013) using a
554 regional South Georgia model, suggested that up to 8 µmol Fe m^{-2} d^{-1} are delivered to the
555 bloom regions downstream of South Georgia by dry and wet deposition. However, reliable
556 dry and wet deposition estimates for the Southern Ocean are limited. Data from the South
557 Atlantic along 40°S, ~ 1.000 km north of South Georgia, showed that rather low levels of
558 DFe (~ 0.002 µmol m^{-2} d^{-1}) are supplied by dry deposition (Chance et al., 2015). In addition,
559 ~ 1.0 ± 1.2 µmol DFe m^{-2} d^{-1} are delivered sporadically to the 40°S area by wet deposition
560 (Chance et al., 2015). However, even when assuming that similar wet deposition fluxes
561 occur north of South Georgia, fertilization with DFe is temporally and spatially limited.
562 Furthermore, it is very unlikely that such sporadic events could cause long-lasting and far
563 extending phytoplankton blooms strictly constrained between the PF and the SACCF.
564
565 3.4.5 Luxury Fe uptake on the shelf

566 Our conservative estimate of DFe supply to the bloom region by vertical/horizontal
567 mixing, deep winter entrainment and dust deposition (< 0.12 µmol Fe m^{-2} d^{-1}) covers only
568 ~30% of the estimated phytoplankton requirements (~ 0.33 µmol Fe m^{-2} d^{-1}) (Fig. 8). We
569 hypothesize that the missing supply of ~ 0.21 µmol DFe m^{-2} d^{-1} is supplied to the bloom
570 region through the off-shore advection of phytoplankton cells that are enriched in labile Fe.
571 It has been demonstrated that Fe-rich biogenic particles can be created by luxury iron uptake
572 of diatoms (Iwade et al., 2006; Marchetti et al., 2009). Using bottle incubation experiments,
573 Iwade et al. (2006) showed that under Fe replete conditions the coastal diatom *Chaetoceros*
574 *sociale* stores more intracellular Fe than needed for the production of essential enzymes and

575 proteins. We therefore hypothesize that phytoplankton cells that grew under excess nutrient
576 supply on the South Georgia shelf stored more Fe than needed for their metabolic processes.
577 Due to subsequent cycles of grazing, lysis or bacterial decomposition, this iron can be
578 remobilised in surface waters and made available for renewed phytoplankton uptake.

579 High Fe recycling efficiencies, described by the f*e* ratio (Boyd et al., 2005), are
580 required to maintain the cycle of remineralisation and uptake in the euphotic zone. This
581 counteracts the loss of particulate Fe by vertical export. Boyd et al. (2015) reported the
582 highest recycling efficiencies of ~ 90% for subantarctic, DFe-deplete waters such as
583 downstream of South Georgia. Further, these workers showed that the degree of recycling is
584 controlled by the abundance of prokaryotes with a high Fe quota, such as cyanobacteria, and
585 particularly by grazing zooplankton. The waters off South Georgia feature among the highest
586 biomasses worldwide of metazoan grazers (Atkinson et al., 2001). These large grazers,
587 chiefly copepods and Antarctic krill, are able to efficiently ingest large diatoms including
588 species that are known to store luxury iron (Atkinson, 1994; Hamm et al., 2003), thereby
589 disintegrating cell membranes and releasing trace metals.

590 In recent years it has become apparent that the recycling of biogenic particles in the
591 euphotic zone is a critical mechanism that maintains primary production, especially when the
592 dissolved nutrient pools become exhausted (Boyd et al., 2015; Tagliabue et al., 2014).
593 However, uncertainties remain over the degree to which Fe is lost during each cycle of uptake
594 and remineralisation. Thus more research is needed, especially field work that encompasses
595 the community structures (bacteria, phytoplankton, zooplankton, and higher predators
596 (Ratnarajah et al., 2017; Wing et al., 2014)), the degree of recycling for macro- and micro-
597 nutrients in the euphotic zone, and loss of Fe through vertical export.

598 An alternative explanation to our suggestion that recycling of luxury iron enriched
599 biota contributes to the downstream bloom is that iron is adsorbed directly onto particles that

600 are advected directly offshore. For example freshly precipitated Fe(III) oxyhydroxides
601 (FeOOH * nH_2O) may be adsorbed onto biogenic and non-biogenic material. Iron freshly
602 absorbed onto biogenic and non-biogenic material can be released and incorporated by
603 phytoplankton and bacteria. However, the bioavailability of adsorbed and inorganic Fe
604 changes over time. Both Wells et al. (1991) and Chen and Wang (2001) demonstrated that
605 the bioavailability of freshly precipitated FeOOH and Fe adsorbed onto colloids/inorganic
606 particles decreases over time. This is primarily due to the dehydration of the loosely packed
607 structure that is subsequently transferred into amorphous FeOOH in the mineral structure
608 Goethite. Because of this we suggest that the majority of Fe from inorganic FeOOH or Fe
609 adsorbed onto particles must be released and utilized in an early stage of the voyage, mainly
610 on the shelf or shortly after the shelf break.
611
612 3.4.6 Budget uncertainties
613 Estimates for Fe budgets are challenging and often contain large uncertainties. This is
614 primarily due to the lack of site- and time-specific flux data. Moreover, the mean annual
615 estimates, necessary for reliable supply calculations, reach a high level of accuracy only after
616 the same region has been monitored multiple times to cover seasonal and annual anomalies.
617 In the following, we will discuss the uncertainty of the different Fe fluxes in the blooming
618 region north of South Georgia.
619 We identified three main processes that account together for ~98% of the total Fe flux
620 in the blooming region, and thus contribute largest uncertainties; the horizontal flux, dry/wet
621 deposition, and winter entrainment. Horizontal flux estimates of this study rely on literature
622 values that were collected offshore the Antarctic Peninsula. In contrast, South Georgia is an
623 island with a confined shelf region and thus horizontal DFe fluxes may differ greatly.
624 Furthermore, we showed that dry deposition dust fluxes are generally low, but showed in

addition that the Fe flux can be supplemented strongly by sporadic wet deposition events (~ 1.0 ± 1.2 µmol DFe m^{-2} d^{-1}) (Chance et al., 2015). Atmospheric fluxes are variable, illustrated by the large standard deviation of the wet deposition Fe fluxes obtained at 40°S. Furthermore, to determine the magnitude of the seasonal DFe winter entrainment reliable estimates of the winter mixing layer depth (WMLD) and the ferrocline are required. Even though the WMLD can be estimated very precisely using Argo float data, the depth of ferrocline in the manuscript of Tagliabue et al. (2014) is based on 140 unique observations distributed over the entire Southern Ocean. Due to this regional anomalies are not captured. In addition to the DFe fluxes in the blooming region, we also assume that the biological Fe demand estimated for the phytoplankton community contributes a large error. The biological Fe requirements were determined using satellite derived net primary production data and an average intracellular Fe/C ratio derived from 5 different diatom species native to the Southern Ocean. Both parameters are not well constrained and because of the lack of observational data we applied the lowest intracellular Fe/C ratio available in the literature (Strzepek et al., 2011). However, we found that even small changes of the both parameters change the estimated Fe availability in the bloom region strongly. Nevertheless, flux estimates even with large uncertainties can help us understand the degree of the nutrient supply vs. consumption by organisms and help to pinpoint the limitation of the estimates made. To ultimately reduce the level of uncertainty and to improve our biogeochemical models more observational data from the bloom region north of South Georgia is required.

4. Conclusions

Shelf sediment-derived Fe and Fe released from Antarctic krill significantly contribute to the DFe distribution in the shelf waters around South Georgia. Nevertheless, DFe enriched in shelf waters are not effectively advected to the phytoplankton bloom region

downstream of the island. Together with other Fe supplies, such as aeolian dust, deep winter mixing and diapycnal mixing, the horizontal advection contributes only ~30% to the Fe requirements of a phytoplankton bloom downstream of South Georgia. We therefore hypothesize that the majority of the Fe is derived from remineralisation of Fe enriched phytoplankton cells and biogenic particles that are transported with the water masses into the bloom region.

While we highlight the importance of grazers and the cycling of various particulate Fe phases in the Fe-fertilisation of the South Georgia bloom, more work is needed to clarify the transport mechanisms of dissolved and particulate Fe.

Author contribution

CS, KS, EPA, SF, and AAt designed the experiments for JC247. CS, MDP and AAt performed the sampling and krill incubation experiments during JC247. CS and MC analysed the trace metal samples at NOCS. EPA sampled the seawater during JC274. Samples from JC274 were analysed by CS and MC. AAq, WBH and RM designed the experiments for JR55 and AAq analysed the samples. CS prepared the manuscript with contributions from all co-authors.

Acknowledgements

We would like to thank the officers and crew of RRS *James Clark Ross* for assistance with the pelagic sampling and those of RRS *James Cook* for the benthic coring. In addition, we thank the two anonymous reviewers for reviewing the manuscript. This work forms part of the NERC-AFI grant AFI9/07 to AA and EA (NE/F01547X/1). RAM was funded by NERC grants NE/01249X/1 and NE/H004394/1. WBH was supported by NERC fellowship NE/K009532/1

675 **References**

676 Achterberg, E. P., Steigenberger, S., Marsay, C. M., LeMoigne, F. A. C., Painter, S. C.,
677 Baker, A. R., Connelly, D. P., Moore, C. M., Tagliabue, A., and Tanhua, T.: Iron
678 Biogeochemistry in the High Latitude North Atlantic Ocean, Scientific Reports, 8(1283), 1-
679 12, 2018.
680 Atkinson, A.: Diets and feeding selectivity among the epipelagic copepod community near
681 South Georgia in summer, Polar Biol., 14, 551-560, 1994.
682 Atkinson, A., Whitehouse, M. J., Priddle, J., Cripps, G. C., Ward, P., and Brandon, M. A.:
683 South Georgia, Antarctica: a productive, cold water, pelagic ecosystem, Mar. Ecol.-Prog.
684 Ser., 216, 279-308, 2001.
685 Berger, C. J. M., Lippiatt, S. M., Lawrence, M. G., and Bruland, K. W.: Application of a
686 chemical leach technique for estimating labile particulate aluminum, iron, and manganese in
687 the Columbia River plume and coastal waters off Oregon and Washington, J. Geophys. Res.,
688 113, 1-16, 2008.
689 Bonneville, S., Behrends, T., and Van Cappellen, P.: Solubility and dissimilatory reduction
690 kinetics of iron(III) oxyhydroxides: A linear free energy relationship, Geochim. Cosmochim.
691 Act., 73, 5273-5282, 2009.
692 Borrione, I., Aumont, O., Nielsdottir, M. C., and Schlitzer, R.: Sedimentary and atmospheric
693 sources of iron around South Georgia, Southern Ocean: a modelling perspective,
694 Biogeosciences Discuss., 10, 10811-10858, 2013.
695 Boudreau, B. P. and Scott, M. R.: A model for the diffusion-controlled growth of deep-sea
696 manganese nodules, Americ. J. Sc., 278, 903-929, 1978.
697 Boyd, P. W., Law, C. S., Hutchins, D. A., Abraham, E. R., Croot, P. L., Ellwood, M., Frew,
698 R. D., Hadfield, M., Hall, J., Handy, S., Hare, C., Higgins, J., Hill, P., Hunter, K. A.,
699 LeBlanc, K., Maldonado, M. T., McKay, R. M., Mioni, C., Oliver, M., Pickmere, S.,

Pinkerton, M., Safi, K., Sander, S., Sanudo-Wilhelmy, S. A., Smith, M., Strzepek, R., Tovar-Sanchez, A., and Wilhelm, S. W.: FeCycle: Attempting an iron biogeochemical budget from a mesoscale SF6 tracer experiment in unperturbed low iron waters, Global Biogeochem. Cycles, 19, 1-13, 2005.

Boyd, P. W., Strzepek, R. F., Ellwood, M. J., Hutchins, D. A., Nodder, S. D., Twining, B. S., and Wilhelm, S. W.: Why are biotic iron pools uniform across high- and low-iron pelagic ecosystems?, Global Biogeochem. Cycles, 29, 1028-1043, 2015.

Browning, T. J., Bouman, H. A., Henderson, G. M., Mather, T. A., Pyle, D. M., Schlosser, C., Woodward, E. M. S., and Moore, C. M.: Strong responses of Southern Ocean phytoplankton communities to volcanic ash, Geophys. Res. Lett., 41, 1-7, 2014.

Buesseler, K. O., Andrews, J. E., Pike, S. M., and Charette, M. A.: The Effects of Iron Fertilization on Carbon Sequestration in the Southern Ocean, Science, 304, 414-417, 2004.

Canfield, D. E. and Thamdrup, B.: Towards a consistent classification scheme for geochemical environments, or, why we wish the term 'suboxic' would go away, Geobiol., 7, 385-392, 2009.

Cassar, N., Bender, M. L., Barnett, B. A., Fan, S., Moxim, W. J., Levy II, H., and Tilbrook, B.: The Southern Ocean Biological Response to Aelian Iron Input, Science, 317, 1067-1070, 2007.

Chance, R., Jickells, T. D., and Baker, A. R.: Atmospheric trace metal concentrations, solubility and deposition fluxes in remote marine air over the south-east Atlantic, Mar. Chem., 177, 45-55, 2015.

Charette, M. A., Gonneea, M. E., Morris, P., Statham, P., Fones, G., Planquette, H., Salter, I., and Garabato, A. N.: Radium isotopes as tracers of iron sources fueling a Southern Ocean phytoplankton bloom, Deep-Sea Res. II, 54, 1989-1998, 2007.

724 Chase, Z., Hales, B., Cowles, T., Schwartz, R., and van Geen, A.: Distribution and variability
725 of iron input to Oregon coastal waters during the upwelling season, J. Geophys. Res., 110, 1-
726 14, 2005.
727 Chen, M. and Wang, W.-X.: Bioavailability of natural colloid-bound iron to marine plankton:
728 Influences of colloidal size and aging, Limnol. Oceanogr., 46, 1956-1967, 2001.
729 Conway, T. M., Wolff, E. W., Rothlisberger, R., Mulvaney, R., and Elderfield, H. E.:
730 Constraints on soluble aerosol iron flux to the Southern Ocean at the Last Glacial Maximum,
731 Nat. Commun., 6, 1-9, 2015.
732 de Boyer Montégut, C., Madec, G., Fischer, A. S., Lazar, A., and Iudicone, D.: Mixed layer
733 depth over the global ocean: An examination of profile data and a profile-based climatology,
734 J. Geophys. Res., 109, 1-20, 2004.
735 de Jong, J., Schoemann, V., Lannuzel, D., Croot, P., de Baar, H. J. W., and Tison, J. L.:
736 Natural iron fertilization of the Atlantic sector of the Southern Ocean by continental shelf
737 sources of the Antarctic Peninsula, J. Geophys. Res., 117, 1-25, 2012.
738 Fielding, S., Watkins, J. L., Trathan, P. N., Enderlein, P., Waluda, C. M., Stowasser, G.,
739 Tarling, G. A., and Murphy, E. J.: Interannual variability in Antarctic krill (Euphausia
740 superba) density at South Georgia, Southern Ocean: 1997–2013, ICES J. Mar. Sci., 2014. 1-
741 11, 2014.
742 Fitzsimmons, J. N. and Boyle, E. A.: Both soluble and colloidal iron phases control dissolved
743 iron variability in the tropical North Atlantic Ocean, Geochim. Cosmochim. Act., 125, 539-
744 550, 2014.
745 Gabric, A. J., Cropp, R. A., McTainsh, G. H., Johnston, B. M., Butler, H., Tilbrook, B., and
746 Keywood, M.: Australian dust storms in 2002 and 2003 and their impact on Southern Ocean
747 biogeochemistry, Global Biogeochem. Cycles, 24, 1-17, 2010.

748 Gao, Y., Kaufman, Y. J., Tanré, D., Kolber, D., and Falkowski, P. G.: Seasonal distributions
749 of aeolian iron fluxes to the global ocean, Geophys. Res. Lett., 28, 29-32, 2001.
750 Gassó, S. and Stein, A. F.: Does dust from Patagonia reach the sub-Antarctic Atlantic
751 Ocean?, Geophys. Res. Lett., 34, 1-5, 2007.
752 German, C. R., Casciotti, K. A., Dutay, J.-C., Heimbürger, L. E., Jenkins, W. J., Measures, C.
753 I., Mills, R. A., Obata, H., Schlitzer, R., Tagliabue, A., Turner, D. R., and Whitby, H.:
754 Hydrothermal impacts on trace element and isotope ocean biogeochemistry, Philos Trans A
755 Math Phys Eng Sci, 374, 1-19, 2016.
756 Gerringa, L. J. A., Alderkamp, A.-C., Laan, P., Thuróczy, C.-E., De Baar, H. J. W., Mills, M.
757 M., van Dijken, G. L., van Haren, H., and Arrigo, K. R.: Iron from melting glaciers fuels the
758 phytoplankton blooms in Amundsen Sea (Southern Ocean): Iron biogeochemistry, Deep-Sea
759 Res. II, 71-76, 16-31, 2012.
760 Giering, S. L. C., Steigenberger, S., Achterberg, E. P., Sanders, R., and Mayor, D. J.:
761 Elevated iron to nitrogen recycling by mesozooplankton in the Northeast Atlantic Ocean,
762 Geophys. Res. Lett., 39, L12608, 2012.
763 Gilpin, L. C., Priddle, J., Whitehouse, M. J., Savidge, G., and Atkinson, A.: Primary
764 production and carbon uptake dynamics in the vicinity of South Georgia-balancing carbon
765 fixation and removal, Mar. Ecol. Prog. Ser., 242, 51-62, 2002.
766 Hamm, C. E., Merkel, R., Springer, O., Jurkojc, P., Maier, C., Prechtel, K., and Smetacek, V.:
767 Architecture and material properties of diatom shells provide effective mechanical protection,
768 Nature, 421, 841-843, 2003.
769 Ho, T.-Y., Quigg, A., Finkel, Z. V., Milligan, A. J., Wyman, K., Falkowski, P. G., and Morel,
770 F. M. M.: The elemental composition of some marine phytoplankton, J. Phycol., 39, 1145-
771 1159, 2003.

772 Homoky, W. B., Hembury, D. J., Hepburn, L. E., Mills, R. A., Statham, P. J., Fones, G. R.,
773 and Palmer, M. R.: Iron and manganese diagenesis in deep sea volcanogenic sediments and
774 the origins of pore water colloids, Geochim. Cosmochim. Act., 75, 5032-5048, 2011.
775 Homoky, W. B., Severmann, S., McManus, J., Berelson, W. M., Riedel, T. E., Statham, P. J.,
776 and Mills, R. A.: Dissolved oxygen and suspended particles regulate the benthic flux of iron
777 from continental margins, Mar. Chem., 134–135, 59-70, 2012.
778 Homoky, W. B., Weber, T., Berelson, W. M., Conway, T. M., Henderson, G. M., van Hulten,
779 M., Jeandel, C., Severmann, S., and Tagliabue, A.: Quantifying trace element and isotope
780 fluxes at the ocean–sediment boundary: a review, Philos Trans A Math Phys Eng Sci, 374,
781 2016.
782 Hutchins, D. A. and Bruland, K. W.: Grazer-mediated regeneration and assimilation of Fe, Zn
783 and Mn from planktonic prey, Mar. Ecol.-Prog. Ser., 110, 259-269, 1994.
784 Iwade, S., Kuma, K., Isoda, Y., Yoshida, M., Kudo, I., Nishioka, J., and Suzuki, K.: Effect of
785 high iron concentrations on iron uptake and growth of a coastal diatom Chaetoceros sociale,
786 Aquat. Microb. Ecol., 43, 177-191, 2006.
787 Jones, E. M., Bakker, D. C. E., Venables, H. J., and Hardman-Mountford, N. J.: Seasonal
788 cycle of CO2 from the sea ice edge to island blooms in the Scotia Sea, Southern Ocean, Mar.
789 Chem., 177, 490-500, 2015.
790 Jones, E. M., Bakker, D. C. E., Venables, H. J., and Watson, A. J.: Dynamic seasonal cycling
791 of inorganic carbon downstream of South Georgia, Southern Ocean, Deep-Sea Res. II, 59–60,
792 25-35, 2012.
793 Kalnejais, L. H., Martin, W. R., and Bothner, M. H.: The release of dissolved nutrients and
794 metals from coastal sediments due to resuspension, Mar. Chem., 121, 224-235, 2010.
795 Klar, J. K., Homoky, W. B., Statham, P. J., Birchill, A. J., Harris, E. L., Woodward, E. M. S.,
796 Silburn, B., Cooper, M. J., James, R. H., Connelly, D. P., Chever, F., Lichtschlag, A., and

797 Graves, C.: Stability of dissolved and soluble Fe(II) in shelf sediment pore waters and release
798 to an oxic water column, Biogeochemistry, 2017. 1-19, 2017.
799 Korb, R. E., Whitehouse, M. J., and Ward, P.: SeaWiFS in the southern ocean: spatial and
800 temporal variability in phytoplankton biomass around South Georgia, Deep-Sea Res. II, 51,
801 99-116, 2004.
802 Koschinsky, A., Winkler, A., and Fritsche, U.: Importance of different types of marine
803 particles for the scavenging of heavy metals in the deep-sea bottom water, Appl Geochem,
804 18, 693-710, 2003.
805 Kurapov, A. L., Allen, J. S., and Egbert, G. D.: Combined Effects of Wind-Driven Upwelling
806 and Internal Tide on the Continental Shelf, Journal of Physical Oceanography, 40, 737-756,
807 2010.
808 Lam, P. J. and Bishop, J. K. B.: The continental margin is a key source of iron to the HNLC
809 North Pacific Ocean, Geophys. Res. Lett., 35, 1-5, 2008.
810 Liu, X. and Millero, F. J.: The solubility of iron in seawater, Mar. Chem., 77, 43-54, 2002.
811 Ma, S., Tao, Z., Yang, X., Yu, Y., Zhou, X., M, W., and Li, Z.: Estimation of marine primary
812 productivity from satellite-derived phytoplankton absorption data, IEEE J-STARS, 7, 3084-
813 3092, 2014.
814 Marchetti, A., Parker, M. S., Moccia, L. P., Lin, E. O., Arrieta, A. L., Ribalet, F., Murphy, M.
815 E. P., Maldonado, M. T., and Armbrust, E. V.: Ferritin is used for iron storage in bloom-
816 forming marine pennate diatoms, Nature, 457, 467-470, 2009.
817 Marsay, C. M., Sedwick, P. N., Dinniman, M. S., Barrett, P. M., Mack, S. L., and
818 McGillicuddy, D. J.: Estimating the benthic efflux of dissolved iron on the Ross Sea
819 continental shelf, Geophys. Res. Lett., 41, 7576-7583, 2014.

820 Meredith, M. P., Brandon, M. A., Murphy, E. J., Trathan, P. N., Thorpe, S. E., Bone, D. G.,
821 Chernyshkov, P. P., and Sushin, V. A.: Variability in hydrographic conditions to the east and
822 northwest of South Georgia, 1996–2001, J. Marine Syst., 53, 143-167, 2005.
823 Milne, A., Schlosser, C., Wake, B. D., Achterberg, E. P., Chance, R., Baker, A. R., Forryan,
824 A., and Lohan, M. C.: Particulate phases are key in controlling dissolved iron concentrations
825 in the (sub)tropical North Atlantic, Geophys. Res. Lett., 44, 2377-2387, 2017.
826 Moore, W. S.: Determining coastal mixing rates using radium isotopes, Cont. Shelf Res., 20,
827 1993-2007, 2000.
828 Murphy, E. J., Trathan, P. N., Watkins, J. L., Reid, K., Meredith, M. P., Forcada, J., Thorpe,
829 S. E., Johnston, N. M., and Rothery, P.: Climatically driven fluctuations in Southern Ocean
830 ecosystems, P ROY SOC B-BIOL SCI, 274, 3057-3067, 2007.
831 Nielsdóttir, M. C., Bibby, T. S., Moore, C. M., Hinz, D. J., Sanders, R., Whitehouse, M.,
832 Korb, R., and Achterberg, E. P.: Seasonal and spatial dynamics of iron availability in the
833 Scotia Sea, Mar. Chem., 130–131, 62-72, 2012.
834 Pakhomova, S. V., Hall, P. O. J., Kononets, M. Y., Rozanov, A. G., Tengberg, A., and
835 Vershinin, A. V.: Fluxes of iron and manganese across the sediment–water interface under
836 various redox conditions, Mar. Chem., 107, 319-331, 2007.
837 Planquette, H., Sanders, R., Statham, P. J., Morris, P. J., and Fones, G. R.: Fluxes of
838 particulate iron from the upper ocean around the Crozet Islands: A naturally iron-fertilized
839 environment in the Southern Ocean, Global Biogeochem. Cycles, 25, 1-12, 2011.
840 Planquette, H., Statham, P. J., Fones, G. R., Charette, M. A., Moore, C. M., Salter, I.,
841 Nedelec, F. H., Taylor, S. L., French, M., Baker, A. R., Mahowald, N., and Jickells, T. D.:
842 Dissolved iron in the vicinity of the Crozet Islands, Southern Ocean, Deep-Sea Res. II, 54,
843 1999-2019, 2007.

844 Pollard, R. T., Salter, I., Sanders, R. J., Lucas, M. I., Moore, C. M., Mills, R. A., Statham, P.
845 J., Allen, J. T., Baker, A. R., Bakker, D. C. E., Charette, M. A., Fielding, S., Fones, G. R.,
846 French, M., Hickman, A. E., Holland, R. J., Hughes, J. A., Jickells, T. D., Lampitt, R. S.,
847 Morris, P. J., Nedelec, F. H., Nielsdottir, M., Planquette, H., Popova, E. E., Poulton, A. J.,
848 Read, J. F., Seeyave, S., Smith, T., Stinchcombe, M., Taylor, S., Thomalla, S., Venables, H.
849 J., Williamson, R., and Zubkov, M. V.: Southern Ocean deep-water carbon export enhanced
850 by natural iron fertilization, Nature, 457, 577-580, 2009.
851 Raiswell, R., Benning, L. G., Tranter, M., and Tulaczyk, S.: Bioavailable iron in the Southern
852 Ocean: the significance of the iceberg conveyor belt, Geochemical Transactions, 9, 1-9, 2008.
853 Raiswell, R. and Canfield, D. E.: The Iron Biogeochemical Cycle Past and Present,
854 Geochemical Perspectives, 1, 1-2, 2012.
855 Rapp, I., Schlosser, C., Rusiecka, D., Gledhill, M., and Achterberg, E. P.: Automated
856 preconcentration of Fe, Zn, Cu, Ni, Cd, Pb, Co, and Mn in seawater with analysis using high-
857 resolution sector field inductively-coupled plasma mass spectrometry, Anal. Chimi. Acta,
858 976, 1-13, 2017.
859 Ratnarajah, L., Lannuzel, D., Townsend, A. T., Meiners, K. M., Nicol, S., Friedlaender, A.
860 S., and Bowie, A. R.: Physical speciation and solubility of iron from baleen whale faecal
861 material, Mar. Chem., 2017. 2017.
862 Sato, M., Takeda, S., and Furuya, K.: Iron regeneration and organic iron(III)-binding ligand
863 production during in situ zooplankton grazing experiment, Mar. Chem., 106, 471-488, 2007.
864 Schlosser, C., De La Rocha, C. L., and Croot, P. L.: Effects of iron surface adsorption and
865 sample handling on iron solubility measurements, Mar. Chem., 127, 48-55, 2011.
866 Schmidt, K., Atkinson, A., Steigenberger, S., Fielding, S., Lindsay, M. C. M., Pond, D. W.,
867 Tarling, G. A., Klevjer, T. A., Allen, C. S., Nicol, S., and Achterberg, E. P.: Seabed foreaging

868 by Antarctic krill: Implications for stock assessment, bentho-pelagic coupling, and the
869 vertical transfer of iron, Limnol. Oceanogr., 56, 1411-1428, 2011.
870 Schmidt, K., Schlosser, C., Atkinson, A., Fielding, S., Venables, H. J., Waluda, C. M., and
871 Achterberg, E. P.: Zooplankton gut passage mobilises lithogenic iron for ocean productivity,
872 Curr. Biol., 26, 1-7, 2016.
873 Strzepek, R., Maldonado, M. T., Hunter, K. A., Frew, R. D., and Boyd, P. W.: Adaptive
874 strategies by Southern Ocean phytoplankton to lessen iron limitation: Uptake of organically
875 complexed iron and reduced cellular iron requirements, Limnol. Oceanogr., 56, 1983-2002,
876 2011.
877 Tagliabue, A., Sallee, J.-B., Bowie, A. R., Levy, M., Swart, S., and Boyd, P. W.: Surface-
878 water iron supplies in the Southern Ocean sustained by deep winter mixing, Nat Geosci, 7,
879 314-320, 2014.
880 Tsuda, A., Saito, H., Machida, R. J., and Shimode, S.: Meso- and microzooplankton
881 responses to an in situ iron fertilization experiment (SEEDS II) in the northwest subarctic
882 Pacific, Deep-Sea Res. II, 56, 2767-2778, 2009.
883 Wedepohl, K. H.: The composition of the continental crust, Geochim. Cosmochim. Act., 59,
884 1217-1232, 1995.
885 Wells, M. L., Mayer, L. M., Donard, O. F. X., Sierra, M. M. D., and Ackelson, S. G.: The
886 Photolysis Of Colloidal Iron In The Oceans, Nature, 353, 248-250, 1991.
887 Whitehouse, M. J., Korb, R. E., Atkinson, A., Thorpe, S. E., and Gordon, M.: Formation,
888 transport and decay of an intense phytoplankton bloom within the High-Nutrient Low-
889 Chlorophyll belt of the Southern Ocean, J. Marine Syst., 70, 150-167, 2008.
890 Wing, S. R., Jack, L., Shatova, O., Leichter, J. J., Barr, D., Frew R. D., and Gault-Ringold,
891 M.: Seabirds and marine mammals redistribute bioavailable iron in the Southern Ocean, Mar.
892 Ecol. Prog. Ser., 510, 1-13, 2014.

Wolanski, E. J. and Delesalle, B.: Upwelling by internal waves, Tahiti, French Polynesia, Cont. Shelf Res., 15, 357-368, 1995.

Yoshida, M., Kuma, K., Iwade, S., Isoda, Y., Takata, H., and Yamada, M.: Effect of aging time on the availability of freshly precipitated ferric hydroxide to costal marine diatoms, Mar. Biol., 149, 379-392, 2006.

Table 1: OTE-seawater samples: Fe, Mn, and Al concentrations determined for the dissolved (D) (0.2 µm) and the leachable particulate fraction (LP_{UN}) (total dissolvable – dissolved) of unfiltered seawater samples collected during JR247. Additional information covers sampling date, site (station) ID, event number and latitude + longitude.

Date	Site ID	Depth	Leach. Part. (nmol L^{-1})			Dissolved (nmol L^{-1})		
	Lat. & Lon.	(m)	$LP_{Un}Fe$	$LP_{Un}Mn$	$LP_{Un}Al$	DFe	DMn	DAl
04/01/2011	#9/10 (E95 & E97)	20	20.36	0.95	46.41	5.71	1.83	1.11
		50	15.18	0.42	40.86	3.19	1.88	2.27
	54.26°S, 35.35°W	100	9.86	0.23	20.43	1.55	0.92	2.07
		130	23.33	0.73	48.91	2.82	0.87	2.68
		150	23.71	0.43	46.95	2.35	1.03	0.12
		200	27.37	0.62	54.41	2.70	0.89	2.37
05/01/2011	#11/12 (E98 & E101)	20	4.05	0.38	6.68	2.19	0.41	3.57
		35	1.52	0.39	7.28	0.41	0.37	-
	54.62°S, 34.81°W	50	9.30	0.60	22.20	7.18	0.64	13.31
		75	1.28	0.31	7.85	0.77	0.35	4.56
		100	2.02	0.32	3.34	1.09	0.35	1.47
		150	1.55	0.38	3.18	1.10	0.45	-
		200	13.10	1.31	23.81	1.26	1.17	3.07
		300	8.62	0.70	23.25	1.06	0.55	-
		400	8.81	0.54	16.54	2.05	0.46	2.69
		500	4.51	0.41	11.41	0.72	0.38	0.76
		600	2.75	0.37	10.32	0.96	0.36	0.77
		700	4.81	0.41	16.85	0.82	0.35	-
06/01/2011	#13 (E105)	20	3.46	0.62	14.68	0.28	0.57	4.53
		35	1.00	0.33	7.17	0.10	0.28	2.64
	54.53°S, 35.27°W	50	7.09	0.71	22.62	1.26	0.57	5.77
		75	25.03	1.09	61.94	1.23	0.64	5.86
		100	34.06	1.30	87.43	0.82	0.74	4.08
07/01/2011	#14 (E113)	20	4.00	0.89	7.87	0.64	0.85	2.57
		50	2.23	0.31	7.64	0.27	0.32	1.80
	54.56°S, 35.59°W	75	2.30	0.43	3.58	0.62	0.46	2.42
		100	2.26	0.44	3.34	0.35	0.46	0.46
		150	23.50	0.94	33.35	0.70	0.62	0.23
		200	82.26	2.12	103.11	2.69	0.77	2.31
08/01/2011	#15/16 (E119 & E129)	20	17.66	0.46	26.66	0.99	1.36	-
		35	16.60	0.30	13.37	0.96	1.27	-
	53.62°S, 36.34°W	50	16.30	0.23	18.49	1.21	1.40	-
		75	23.82	0.56	29.86	0.98	1.28	-
		100	8.49	0.10	10.50	0.73	0.56	-
		150	1.88	0.03	4.49	2.25	0.40	-
		200	2.72	0.02	1.40	0.63	0.44	2.87

		300	2.56	0.05	2.40	0.34	0.25	-
		400	3.75	0.02	5.28	0.48	0.30	1.17
		500	5.28	0.08	9.22	0.43	0.30	-
		600	5.50	0.09	11.45	0.53	0.28	1.63
		750	5.27	0.06	8.16	0.44	0.30	-
10/01/2011	#17 (E133)	20	10.92	0.22	7.43	2.31	1.20	3.76
		35	20.83	0.53	16.22	1.81	1.34	2.56
	53.90°S, 36.57°W	50	34.59	1.00	57.55	2.29	1.42	2.33
		75	118.25	2.18	64.36	4.21	1.86	2.19
		100	50.71	1.00	77.52	2.48	1.42	1.62
		150	112.28	2.23	86.09	3.39	1.41	0.86
11/01/2011	#18 (E138)	20	106.71	1.77	95.17	2.75	1.57	3.36
		35	83.53	0.00	100.32	1.97	1.33	2.44
	54.10°S, 36.25°W	50	9.67	0.00	18.23	0.74	0.85	-
		75	5.65	0.00	8.90	0.62	0.65	-
		100	4.50	0.08	23.65	1.25	0.48	5.18
		150	7.81	0.11	12.87	1.43	0.49	8.19
12/01/2011	#19/20 (E141 & E143)	20	60.19	2.11	54.29	1.46	1.71	5.30
		35	60.17	2.19	87.17	1.34	1.90	8.22
	53.54°S, 38.11°W	50	66.78	2.74	141.75	1.57	1.90	8.73
		75	71.69	1.78	79.19	1.61	2.13	11.45
		100	10.77	0.25	32.12	0.99	0.67	10.74
		150	5.43	0.13	31.35	1.84	0.92	12.00
		200	7.92	0.14	27.42	1.45	0.60	9.60
		400	5.35	0.00	23.61	1.61	0.45	18.44
		600	5.81	0.10	35.99	1.06	0.38	10.74
		800	4.26	0.13	35.67	1.07	0.36	11.95
13/01/2011	#21 (E151)	20	44.75	1.54	114.13	0.72	1.38	2.58
		35	39.99	1.82	73.37	0.77	0.94	2.29
	53.75°S, 38.98°W	50	48.57	2.03	94.66	1.24	1.36	1.91
		75	25.63	0.91	68.56	0.98	1.17	-
		100	64.06	1.91	114.03	2.33	1.32	1.51
		150	73.04	1.59	62.83	7.70	1.28	12.20

903

Table 2: SAPS samples: The particulate Fe (PFe), Mn (PMn), and Al (PAl) concentrations in the top 150 m of the water column at the 14 sites visited during JR247. The particulate fraction, P, is the sum of leachable (L) and refractory (R). Because of low concentrations, the leachable fraction is indicated in percent of the P fraction. Additional information covers sampling date, site (station) ID, event number, latitude and longitude, and water column depth. (Depths marked by * indicate that the polycarbonate filter was corrupted after retrieving the SAPS)

Date	Site ID	Depth	Particulate (nmol L^{-1})			Leach. Part. (% of P)		
	Lat. & Lon.	(m)	PFe	PMn	PAl	LFe	LMn	LAl
25/12/2010	#1/2 (E22)	20	5.17	0.08	4.82	0.37	2.39	1.65
	53.70°S, 38.21°W	50*	9.12	0.14	7.91	0.27	2.61	1.47
	(322 m)	150*	76.61	1.09	66.91	6.26	2.74	4.65
26/12/2010	#3 (E31)	20	6.62	0.09	6.64	0.02	3.30	0.79
	53.85°S, 39.14°W	50	267.48	3.85	162.59	1.48	0.79	0.65
	(287 m)	150	4.36	0.06	4.26	0.07	1.55	1.93
31/12/2010	#4/5 (E72)	20	8.52	0.12	7.99	0.51	1.68	2.62
	53.49°S, 37.71°W	50	15.15	0.23	12.96	0.56	2.44	2.74
	(1917 m)	150	2.33	0.03	2.15	0.65	1.78	2.42
02/01/2011	#6 (E80)	20	85.74	1.11	59.05	1.60	2.28	4.50
	53.99°S, 36.37°W	50	17.76	0.24	8.87	-	-	-
	(208 m)	150	137.39	2.02	98.54	3.46	0.91	2.81
03/01/2011	#7/8 (E88)	20	1.95	0.02	0.87	0.13	2.97	4.99
	54.10°S, 35.46°W	50	1.67	0.02	0.92	0.08	4.35	4.24
	(330 m)	150	1.23	0.02	0.71	0.19	2.11	5.13
04/01/2011	#9/10 (E96)	20	20.91	0.08	15.74	0.56	5.01	3.24
	54.26°S, 35.35°W	50	19.16	0.27	15.58	0.45	1.22	2.51
	(263 m)	150	54.06	0.77	48.10	1.08	1.65	2.08
05/01/2011	#11/12 (E100)	20*	1.49	0.01	0.86	0.18	4.42	2.92
	54.62°S, 34.81°W	50	0.87	0.01	0.60	0.27	6.63	4.20
	(747 m)	150	1.76	0.03	1.08	0.37	4.38	3.33
06/01/2011	#13 (E106)	20	2.75	0.03	1.78	0.63	3.13	4.29
	54.53°S, 35.27°W	50	4.11	0.05	3.07	0.44	2.04	2.76
	(133 m)	100	10.28	0.15	7.62	0.46	1.70	2.54
07/01/2011	#14 (E114)	20	2.80	0.04	1.84	0.07	1.58	3.29
	54.56°S, 35.59°W	50	1.41	0.02	0.97	0.10	2.57	3.92
	(263 m)	150	31.34	0.46	26.92	0.72	1.57	2.28
08/01/2011	#15/16 (E120)	20	24.54	0.37	22.91	0.85	3.95	1.88
	53.62°S, 36.34°W	50	27.72	0.40	23.23	0.43	3.65	1.36
	(852 m)	150	4.74	0.07	3.94	0.90	4.31	1.06

10/01/2011	#17 (E134)	20	10.43	0.14	8.09	0.34	1.66	2.41
	53.90°S, 36.57°W	50	43.04	0.60	38.79	1.34	1.07	1.67
	(209 m)	150	207.48	3.10	194.88	1.72	0.82	1.50
11/01/2011	#18 (E139)	20	95.52	1.32	88.39	1.39	1.82	1.93
	54.10°S, 36.25°W	50	37.43	0.52	35.33	1.16	1.29	1.85
	(276 m)	150	28.00	0.41	23.60	1.26	2.35	2.27
12/01/2011	#19/20 (E142)	20	97.60	1.52	97.10	0.16	1.66	0.33
	53.54°S, 38.11°W	50	90.96	1.42	92.89	0.39	1.98	0.80
	(1741 m)	150	7.41	0.12	6.37	0.74	8.25	2.75
13/01/2011	#21 (E152)	20	50.75	0.85	52.78	0.06	2.99	0.12
	53.75°S, 38.98°W	50	59.59	0.93	59.98	0.05	2.15	0.09
	(269 m)	150	153.48	2.34	89.63	3.14	1.10	2.94

911

912 **Table 3:** Illustrates the different elemental ratios of earth crust, sediment, suspended (SAPS),
913 faecal pellet, and biogenic particles (average phytoplankton species).

particle	Fe/Mn (mol mol^{-1})	Fe/Al (mol mol^{-1})	Mn/Al (mol mol^{-1})	source
crustal	58.00	0.20	0.0035	a
sediment	51.50	0.34	0.0066	This study
suspended (SAPS)	68.00	1.25	0.0171	This study
faecal pellet	70.65	0.48	0.0069	This study
phytoplankton	1.70	-	-	b

914 a) Wedepohl, 1995; b) Ho et al., 2003

915

916 **Table 4: Sediment core samples:** Particulate iron (SFe), aluminum (SAl), and manganese
917 (SMn) concentrations in shelf sediments collected during JC055 in January and February
918 2011. Pore water data retrieved additionally from these three cores are listed for Fe (Fe_{PW})
919 and Mn (Mn_{PW}). Additional information are event number (MC…), latitude + longitude, and
920 water column depth.

Station ID Lat. & Lon.	Depth (cm)	SFe (mol kg-1)	SAl (mol kg-1)	SMn (mmol kg-1)	Fe_{PW} (µmol kg-1)	Mn_{PW} (µmol kg-1)
#S1 (MC33)	0.5	0.58	1.77	11.56	3.01	2.29
54.16°S, 37.98°W	1.5	0.61	1.74	11.52	17.47	0.84
(257 m)	2.5	0.59	1.77	11.78	110.90	0.28
	3.5	0.6	1.86	12.05	106.24	0.53
	4.5	0.58	1.72	11.82	94.09	0.34
	5.5	0.59	1.86	12.04	82.79	0.27
	9	0.56	1.72	11.19	32.98	0.00
	15	0.55	1.74	11.15	2.44	0.06
	25	0.53	1.6	10.81	0.80	0.16
#S2 (MC34)	0.5	0.64	1.77	11.42	1.53	0.87
54.16°S, 37.94°W	1.5	0.6	1.79	11.73	/	/
(247 m)	2.5	0.58	1.76	11.81	0.97	0.24
	6.5	0.59	1.83	12.23	11.19	0.26
	10.5	0.58	1.8	11.78	14.28	0.25
	14.5	0.54	1.6	10.83	3.59	0.33
	16.5	0.56	1.72	11.22	2.27	0.31
#S3 (MC35)	0.5	0.61	1.67	11.42	1.46	0.43
54.15°S, 37.97°W	1.5	0.59	1.76	11.7	28.94	0.35
(254 m)	2.5	0.58	1.76	11.7	91.52	0.37
	3.5	0.59	1.81	12.03	40.16	0.44

5.5	0.57	1.78	11.58	49.37	0.56
8.5	0.59	1.82	11.65	67.92	0.52
17	0.54	1.69	10.8	3.87	0.34
19	0.55	1.67	10.86	1.82	0.12
25	0.55	1.77	11.19	2.73	0.36
29	0.56	1.79	11.19	5.64	0.16

921

Table 5: Krill faecal pellets: Particulate (P) and leachable (L) concentrations for Fe, Mn, and Al determined for the 27 individual krill faecal pellet samples collected during 9 krill incubation experiments on-board RRS *James Clark Ross* (JR247). The particulate fraction, P, is the sum of leachable (L) and refractory (R). Because of low concentrations, the leachable fraction is indicated in percent of the P fraction.

# Sample	pellet weight (mg)	PFe (µg mg^{-1})	PAl (µg mg^{-1})	PMn (ng mg^{-1})	LFe (%)	LAl (%)	LMn (%)
1	4.87	0.88	1.06	12.5	6.33	8.83	13.24
2	2.18	1.33	1.68	16.7	3.02	8.81	8.22
3	4.26	1.07	1.90	17.8	5.37	3.27	11.81
4	1.91	5.19	5.53	76.1	2.15	1.95	5.68
5	1.41	2.70	2.84	39.1	2.46	1.59	3.54
7	7.80	67.1	64.2	998.3	2.93	2.21	3.25
8	0.99	2.71	2.42	35.0	3.76	4.59	5.99
10	1.48	6.42	4.89	71.6	0.29	4.83	0.91
13	2.79	4.13	3.11	50.3	0.36	5.07	1.53
15	0.77	37.3	38.1	531.1	2.03	2.80	6.21
16	1.21	6.35	6.22	81.2	1.24	7.47	3.13
18	12.27	40.0	36.6	582.5	3.95	2.07	4.29
19	2.19	11.2	9.49	146.9	0.15	2.03	1.07
22	2.43	48.1	49.7	721.5	0.81	2.32	0.98
40	3.35	22.8	22.0	337.4	5.51	3.21	5.50
41	8.55	6.91	7.14	103.1	1.11	1.88	4.31
42	3.5	25.7	24.8	376.2	5.09	2.98	5.29
45	0.40	3.96	4.43	43.3	1.27	13.90	1.46
47	7.65	3.63	3.92	52.7	0.34	0.68	3.65
48	0.63	3.06	3.21	34.1	0.05	4.22	0.76
49	4.42	29.6	28.5	438.4	1.65	2.93	1.95
50	7.46	2.31	2.37	34.6	0.36	0.51	2.78
51	5.18	28.0	27.1	431.3	1.85	2.60	2.01
62	1.20	4.63	4.68	68.0	0.31	1.78	0.47
68	2.25	44.0	40.2	667.4	4.84	1.95	4.77
69	1.66	43.6	44.8	663.7	5.66	2.13	5.46
71	3.47	35.3	36.4	557.7	1.50	1.99	1.76

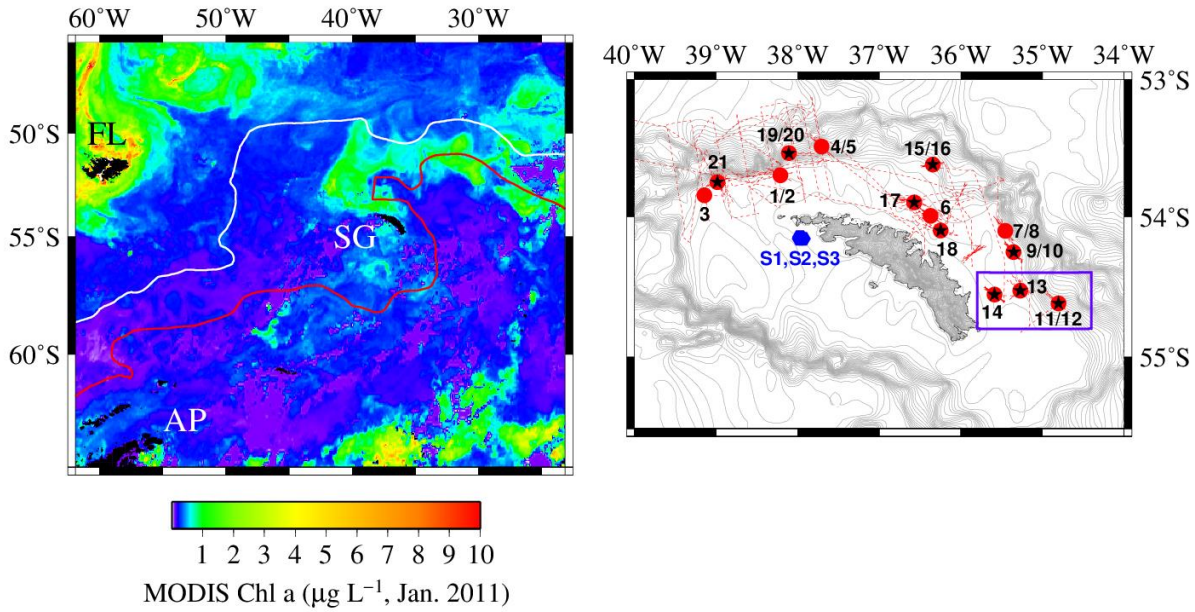

928

929 **Figure 1:** (Left figure) Locations of Falkland Islands (FL), South Georgia (SG), and
930 Antarctic Peninsula (AP) in the Atlantic sector of the Southern Ocean. South Georgia is
931 located between the Antarctic Polar Front (PF, white line) and the Subantarctic Circumpolar
932 Current Front (SACCF, red line). The colour bar represents the Chlorophyll a (Chl a) content
933 recorded by the MODIS satellite in January 2011. (Right figure) The region around SG and
934 the **OTE** (black stars) and **SAPS** sampling sites (red points) visited during JR247. The red
935 dashed line illustrates the cruise track of JR247. The three sediment sampling sites S1, S2,
936 and S3 visited during JC055 are shown by blue hexagons. The purple box indicates the W-E
937 transect from shelf site #14 via site #13 to the shelf edge site #11/12. The ocean bathymetry
938 of the region was plotted using the GEBCO bathymetric data set. The shelf of South Georgia
939 is between 100 and 250 m deep and extends about 30 to 100 km (shelf edge indicated by high
940 density of isobaths).

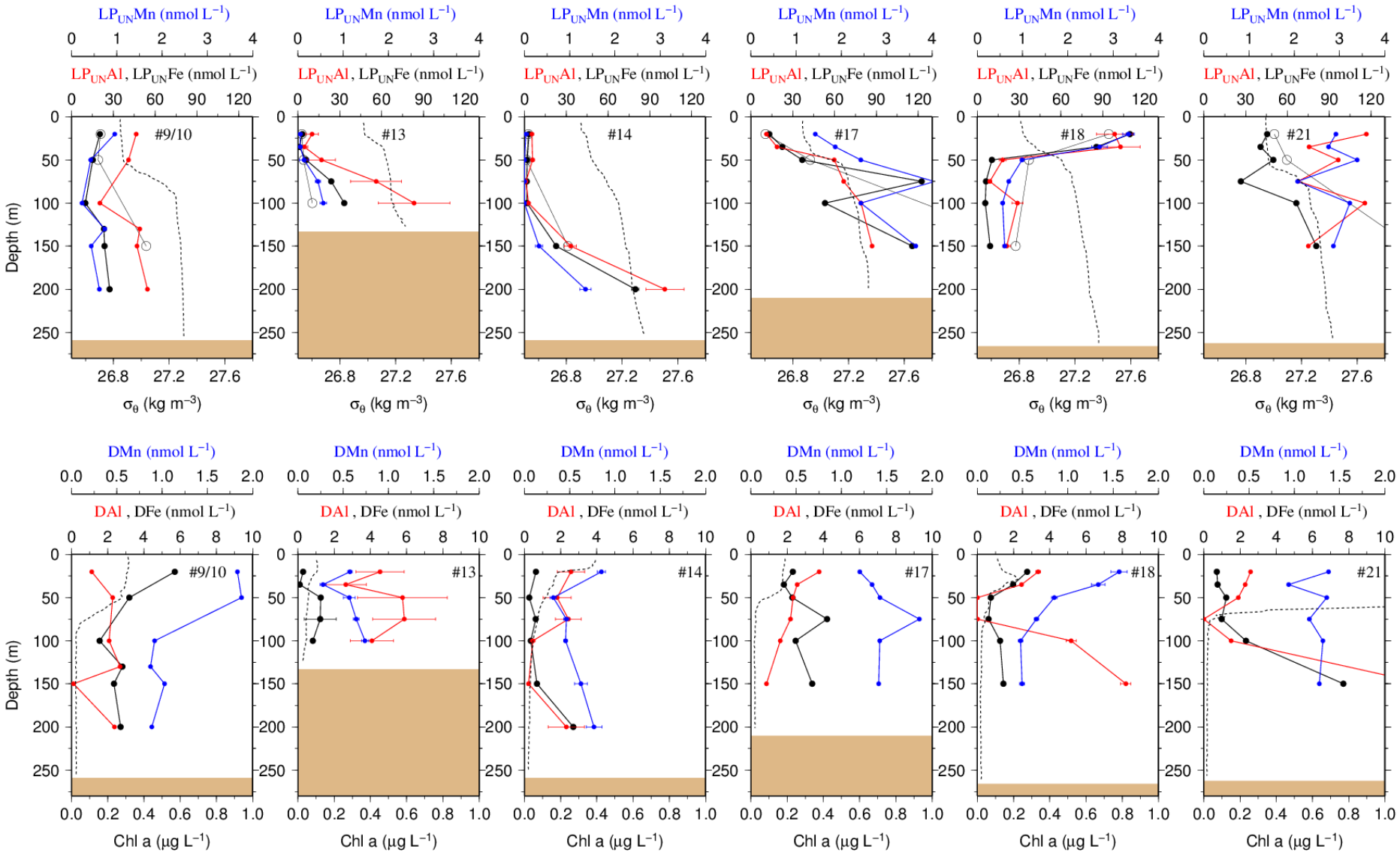
LPUNMn (nmol L−1)
LPUNAl, LPUNFe (nmol L−1)
Depth (m)
σθ (kg m−3)
#9/10
#13
#14
#17
#18
#21
DMn (nmol L−1)
DAl , DFe (nmol L−1)
Chl a (μg L−1)

941

Figure 2: (Upper row) **OTE-seawater samples:** Distribution of leachable particulate iron ($LP_{Un}Fe$ in black), manganese ($LP_{Un}Mn$ in blue), and aluminium ($LP_{Un}Al$ in red) concentrations in the water column of stations located on the island shelf (125 m – 270 m water depth). **SAPS samples:** The particulate Fe (PFe) fraction retrieved by SAPS is illustrated with open black circles and corresponds to the same axis as $LP_{Un}Fe$. Concentrations above 120 nmol L^{-1} are listed in Table 1 and 2. Error bars represent the standard deviation of the analysis. Density sigma-theta (σ_θ) in kg m^{-3} is illustrated by the black dashed line. (Lower row) **OTE-seawater samples:** Dissolved iron (DFe), manganese (DMn), and aluminium (DAl) are represented by the same colour code as above. Dashed lines illustrate Chlorophyll a (Chl a) content of the water column recorded by the CTD fluorometer.

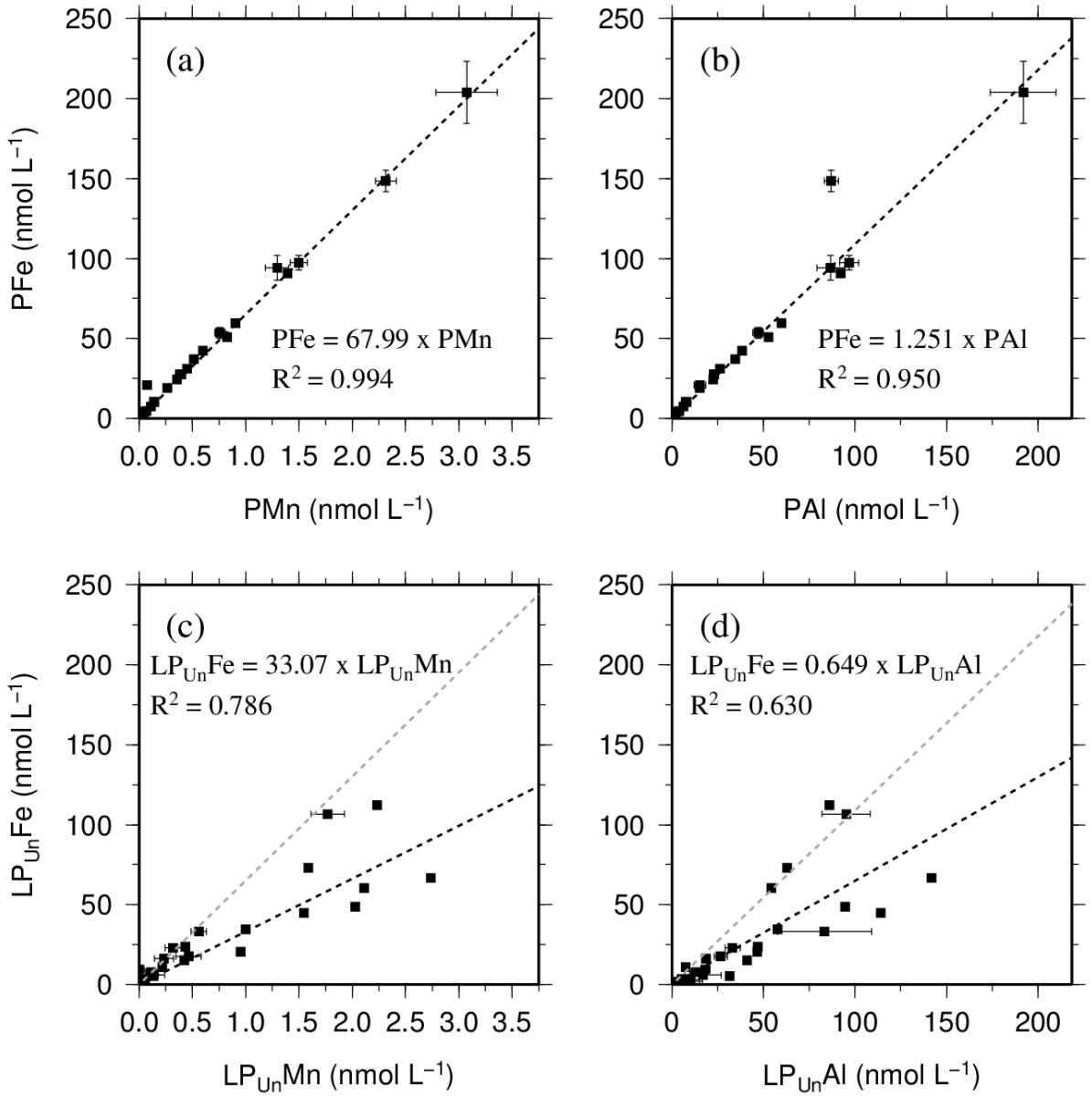

953

954 **Figure 3:** Relationship of the entire data set for the particulate fraction of Fe, Mn, and Al in
955 particulates (P) retrieved using SAPS ((a) and (b)) and the leachable particulate fraction
956 (LP_{UN}) estimated from unfiltered and dissolved seawater samples collected using OTE bottles
957 ((c) and (d)). Error bars represent the standard deviation of the analysis. The linear regression
958 of each relationship is illustrated by a dashed black line, the formula, and the R^2. The grey
959 dashed line in c. and d. represents the linear relationship of particulate trace meals (P) shown
960 in (a) and (b).

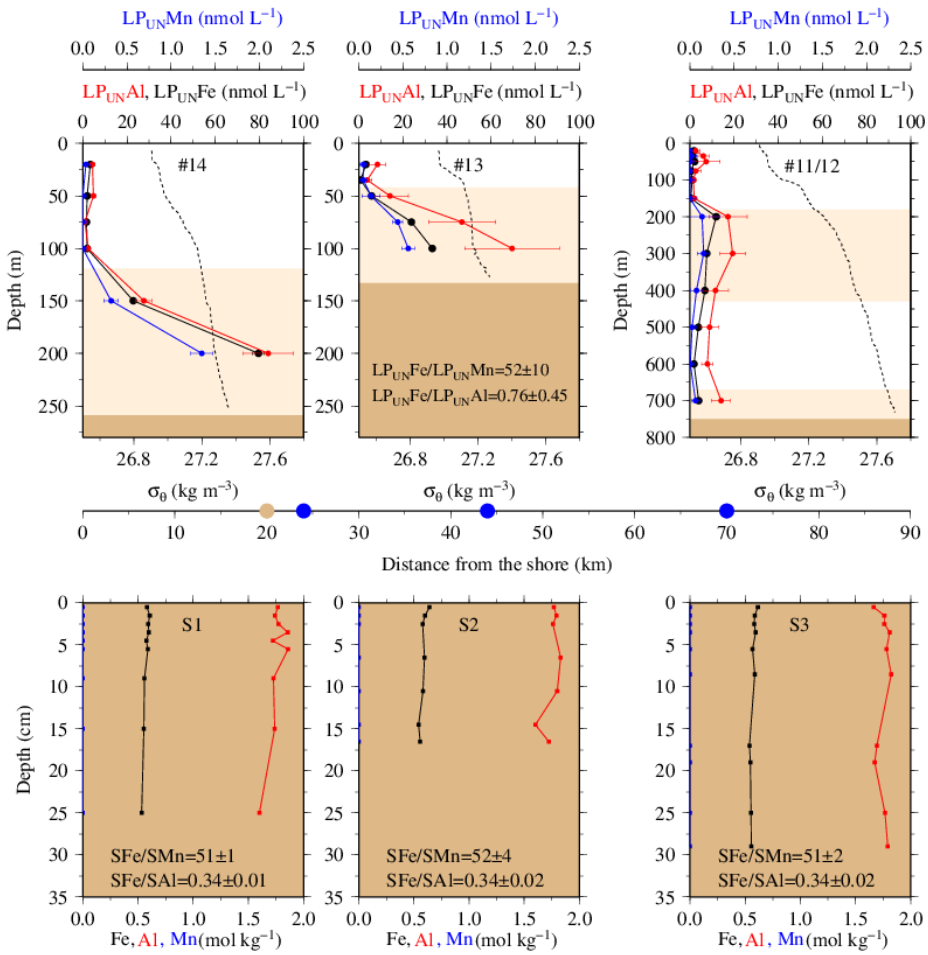

Figure 4: (Upper row) **OTE-seawater samples:** From left to right, concentrations of leachable particulate iron ($LP_{Un}Fe$), aluminium ($LP_{Un}Al$), and manganese ($LP_{Un}Mn$) of unfiltered seawater samples for the two shelf sites #14, #13 and the shelf edge site #11/12 (Note different depth scaling). Error bars represent the standard deviation of the analysis. Water density (sigma-theta (σ_θ)) is shown by the dashed black line. Brown areas represent sediments and pink areas the zone of resuspended sediment particles in the water column. Diagram 14 (left) contains the average $LP_{Un}Fe/LP_{Un}Al$ and $LP_{Un}Fe/LP_{Un}Mn$ ratio of particles in seawater samples collected within the pink layers. (Lower row) **Sediment core samples:** Diagram S1, S2 and, S3 displays the Fe, Mn, and Al content in the three sediment cores. Shown are average SFe/SAl and SFe/SMn ratios (mol/mol) of particles from the surface layer for site S1, S2, and S3. Dots on the distance scaling in the middle represent the distance of each water column station (blue) and sediment core (brown) station to the nearest shore.

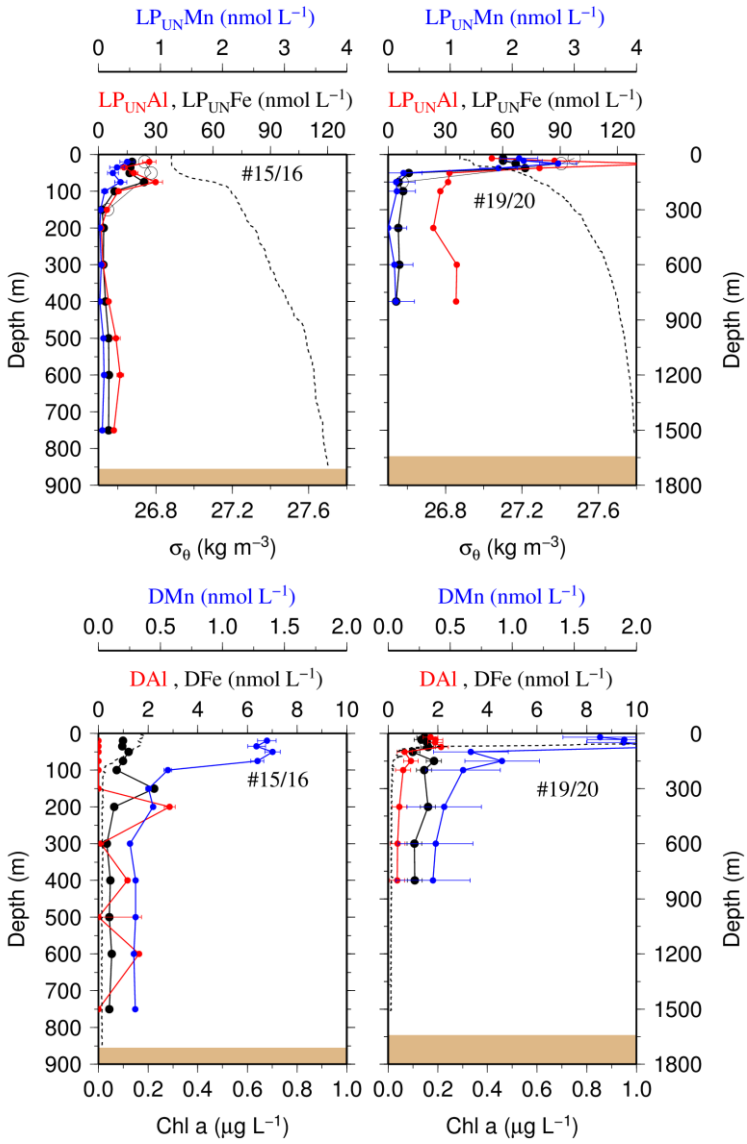

974

975 **Figure 5:** (Upper row) **OTE-seawater samples:** Distribution of leachable particulate
976 manganese ($LP_{Un}Mn$ in blue), iron ($LP_{Un}Fe$ in black), and aluminium ($LP_{Un}Al$ in red)
977 concentrations in the water column of the two other stations located on the island shelf edge
978 (> 700 m water depth). **SAPS samples:** The particulate Fe (PFe) is illustrated by black circles
979 and corresponds to the concentration labels of $LP_{Un}Fe$. Error bars represent the standard
980 deviation of the analysis. Sigma-theta (σ_θ) is illustrated by the black dashed line. (Lower row)
981 **OTE-seawater samples:** Dissolved manganese (DMn), iron (DFe), and aluminium (DAl) are
982 represented by the same colour code as for the upper row. Dashed line illustrates the Chl a
983 content of the water column recorded by the CTD mounted fluorometer.

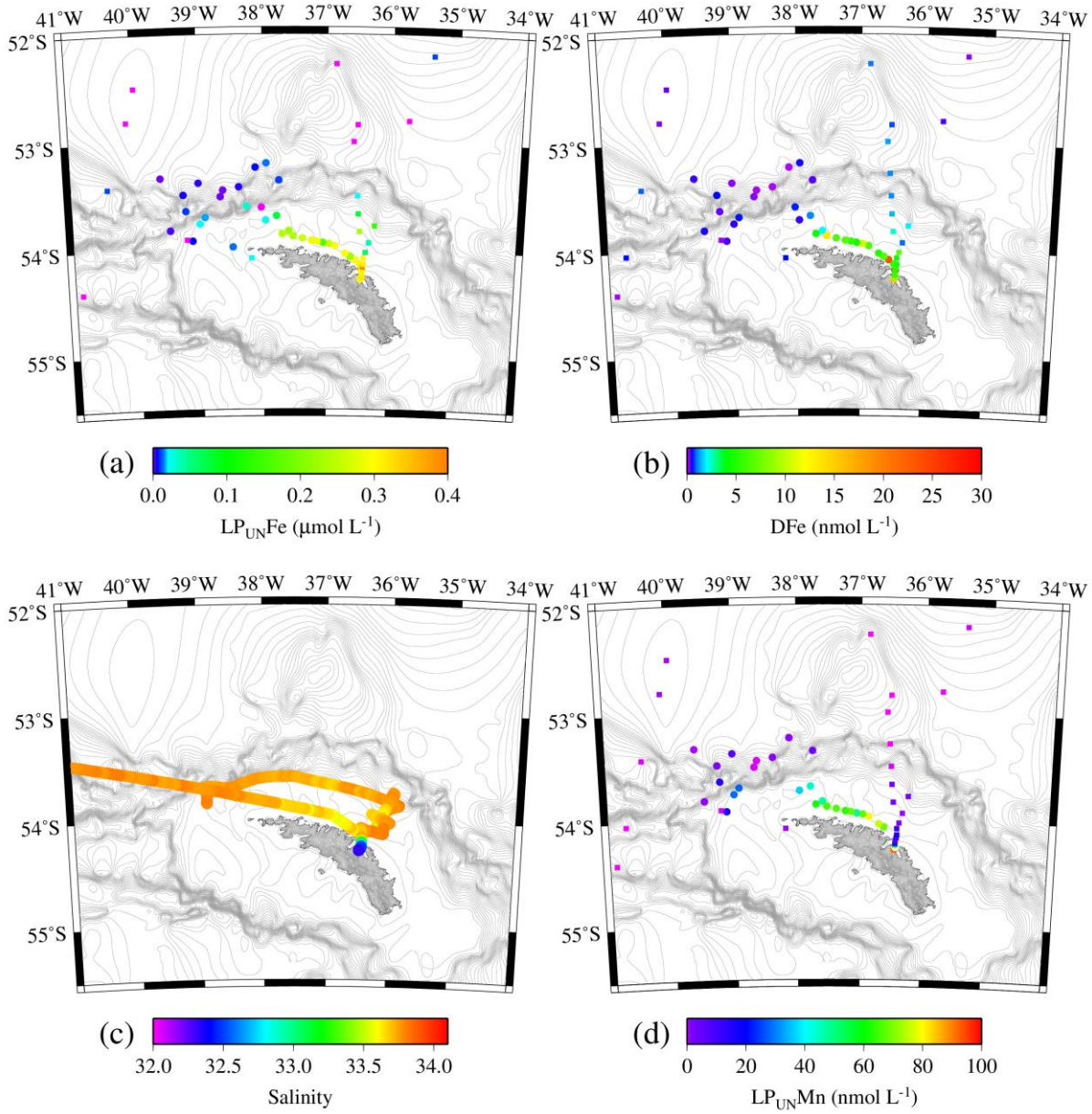

Figure 6: Tow fish-seawater samples: Concentrations of leachable particulate Fe ($LP_{UN}Fe$) of unfiltered seawater samples (a), dissolved Fe (DFe) (b), Salinity (c) and leachable particulate Mn ($LP_{UN}Mn$) in unfiltered seawater samples (d) in surface waters collected during JR247 (circles) and JR274 (squares) around South Georgia. The highest $LP_{UN}Fe$ concentration was recorded in a single sample in Cumberland Bay reaching 2.2 µmol L^{-1}. Because of generally lower concentrations we excluded this data point in panel (a). Isobath are represented by grey lines (GEBCO – Gridded Bathymetry Data).

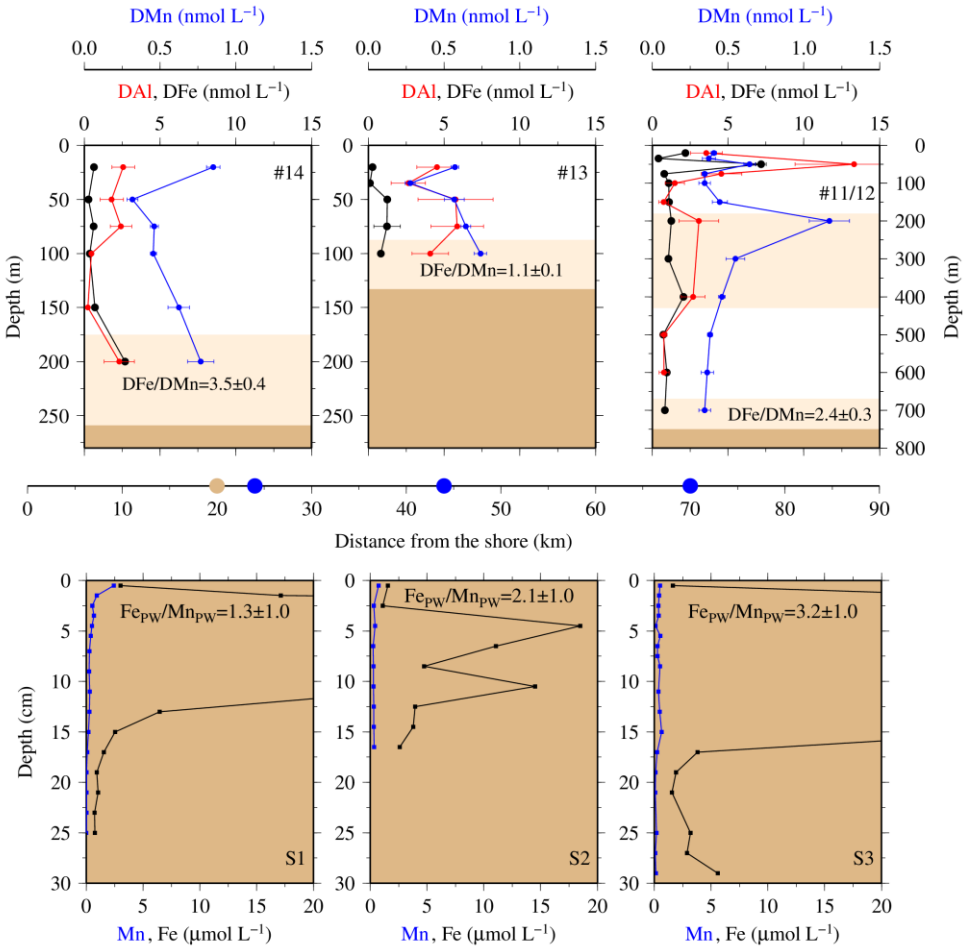

992

993 **Figure 7:** (Upper row) **OTE-seawater samples:** From left to right, concentrations of
994 dissolved iron (DFe), aluminium (DAl), and manganese (DMn) for the two shelf sites (#14,
995 #13) and the shelf edge site (#11/12). Note different depth scaling. Error bars represent the
996 standard deviation of the analysis. Pink areas represent the zone of resuspended sediments in
997 the water column. The DFe/DMn ratios of the seawaters collected within the pink zone is
998 indicated. (Lower row) **Sediment core samples:** Diagram S1, S2 and, S3 displays the Fe
999 (black), and Mn (blue) content in pore waters of the three sediment cores. Values off-axis
1000 can be found in Table 4. Shown are average Fe_{PW}/Mn_{PW} ratios (mol/mol) of top surface layer
1001 (1 cm) for site S1, S2, and S3. Dots on the distance scaling in the middle represent the
1002 distance of each water column station (blue) and sediment core (brown) station to the nearest
1003 shore.

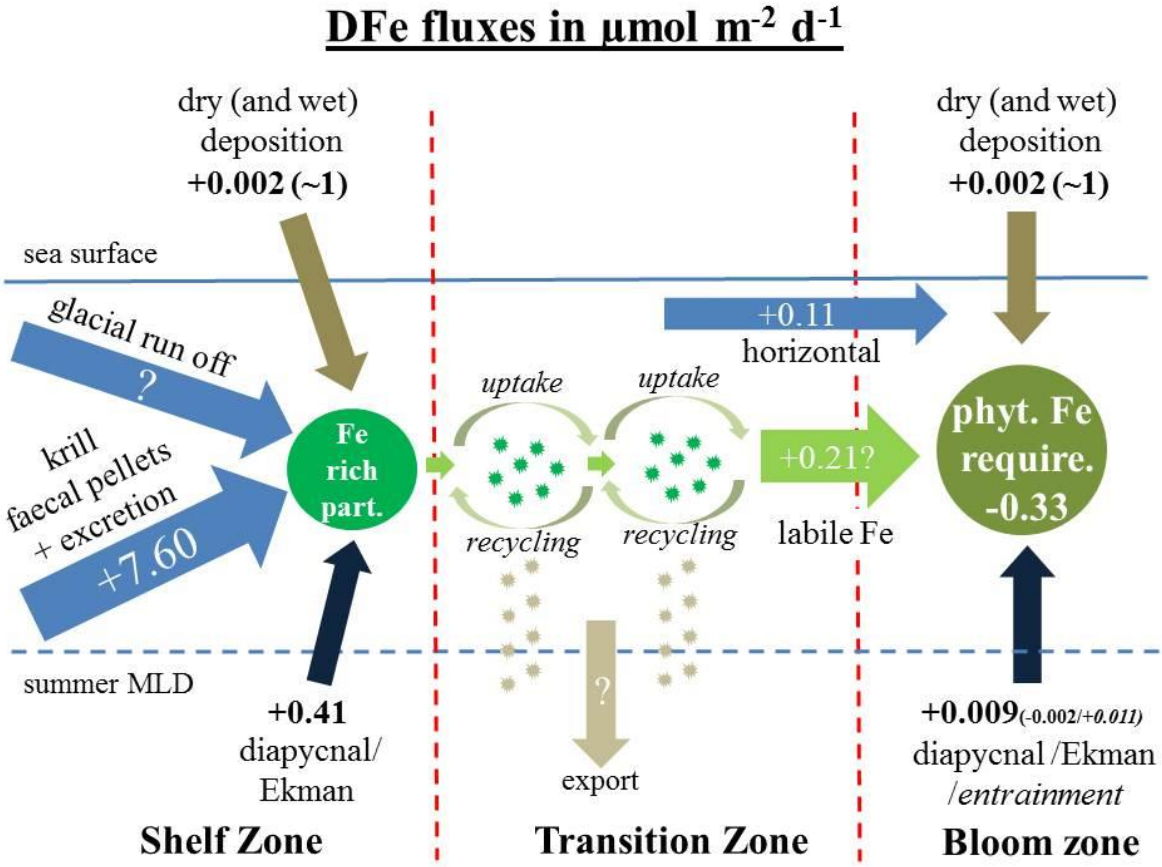

Figure 8: Sketch of DFe fluxes on the shelf, in the transition zone and in the downstream blooming region, separated by the red dashed lines. (left sketch) Describes the dissolved Fe fluxes on the shelf that together generate Fe rich biogenic and lithogenic particles (dark green). These are transferred offshore (light green arrows) following the ACC to open ocean sites (sketch in the middle). Iron enriched particles (dark green) in the transition zone are recycled and supplement DFe requirements of the phytoplankton community in the transition zone. During each cycle of recycling and uptake an unknown Fe fraction is lost by vertical export. (right sketch) Describes the dissolved Fe fluxes in the blooming zone.